Research Square

Preprints are preliminary reports that have not undergone peer review.
They should not be considered conclusive, used to inform clinical practice,
or referenced by the media as validated information.

Histone lactylation-regulated m6A methylase GPR81/METTL3/YTHDC1 accelerates AMPD3-induced ferroptosis in diabetic nephropathy via interaction with HSP90α

Weiwei Zhang
Wannan Medical University, Wannan Medical University
Meng Wang
Wannan Medical University
Xiangjian Meng
The First Affiliated Hospital of Wannan Medical University
Jianbo Ye
Wannan Medical University
Yinping Shui
Wannan Medical University
Qin Yin
Wannan Medical University, Wannan Medical University
Zhichen Pu
puzhichen@wnmc.edu.cn
Wannan Medical University

Research Article

Keywords: histone lactylation, ferroptosis, AMPD3, METTL3, YTHDC1, diabetic nephropathy

Posted Date: November 25th, 2026

DOI: https://doi.org/10.21203/rs.3.rs-11501643/v1

License: This work is licensed under a Creative Commons Attribution 4.0 International License.
Read Full License

Additional Declarations: No competing interests reported.

Histone lactylation-regulated m6A methylase GPR81/METTL3/YTHDC1 accelerates AMPD3-induced ferroptosis in diabetic nephropathy via interaction with HSP90α

Weiwei Zhang[1#], Meng Wang[2#], Xiangjian Meng[3#], Jianbo Ye[2#], Yinping Shui[4*], Qin Yin[1*] and Zhichen Pu5[4*]

[1]Department of Pharmacy, Wannan Medical University, The Second Affiliated Hospital of Wannan Medical University, Wuhu, Anhui 24000, China
[2]College of Pharmacy, Wannan Medical University, Wuhu, Anhui 24000, China
[3]Department of Endocrinology, The First Affiliated Hospital of Wannan Medical University, Wuhu, Anhui 24000, China
[4]Graduate School, Wannan Medical University, Wuhu, Anhui 24000, China
[5]Department of Drug Clinical Evaluation, The First Affiliated Hospital of Wannan Medical University (Yijishan Hospital of Wannan Medical University), Wuhu, Anhui 241001, P. R. China

Corresponding author: Zhichen Pu, Department of Drug Clinical Evaluation, Yijishan Hospital of Wannan Medical College, Wuhu, Anhui 241001, China; Anhui Province Key Laboratory of Non-coding RNA Basic and Clinical Transformation; e-mail: puzhichen@wnmc.edu.cn, phone: +86-15855976176, fax: +86-0553-5738200.
Qin Yin, Department of Pharmacy, Wannan Medical University, The Second Affiliated Hospital of Wannan Medical University, Wuhu, Anhui 24000, China; e-mail: yq0553@163.com;
Yinping Shui, Graduate School, Wannan Medical University, Wuhu, Anhui 24000, China; Tel: (+86)159-0553-0655, e-mail: 20120042@wnmc.edu.cn.

Running title: Histone lactylation/m6A/ METTL3 accelerates AMPD3-induced ferroptosis in Diabetic nephropathy

Abstract

Background: With the development of society, the incidence rate of diabetic nephropathy (DN) has been increasing year by year. However, the underlying mechanisms of lactate's involvement in DN remain unclear. This study attempts to reveal the role and mechanism of Histone lactylation-regulated m6A-methylase on AMPD3 in DN.

Methods: Blood samples were collected from healthy volunteers and DN patients were collected from our hospital. DN mice were fed with a high-fat diet (HFD), and then injected with STZ (streptozotocin). $P < 0.05$ was considered significant and evaluated using Student's t-test or one-way analysis of variance (ANOVA) followed by Tukey's post-test.

Results: The expression and effects of lactate in patients with DN, serum lactate in patients with DN was increased. Inhibition of lactate alleviates DN. The high-lactate microenvironment induced by DN promotes the upregulation of H3K14la in murine renal tissues in model of DN. GPR81/METTL3/YTHDC1 axis mediates AMPD3 mRNA stability through m6A modification by METTL3. METTL3-mediated AMPD3 in lactate-induced ROS accumulation and lipid peroxidation induces ferroptosis via mitochondrial fragmentation in model of DN. AMPD3 induced HSP90a/Drp1 to promote mitochondrial fragmentation by MCU in model of DN. AMPD3 interacted with HSP90a by promoting its K63-linked polyubiquitination and proteasomal degradation in model of DN. Abietic acid (AA) targeting AMPD3 alleviates DN through ferroptosis by mitochondrial fragmentation in model of DN by HSP90a/Drp1.

Conclusions: Our findings suggest that a histone lactylation induces ferroptosis via the GPR81/METTL3/YTHDC1/ AMPD3 axis in renal tubular epithelial during DN. Targeting METTL3/YTHDC1/ AMPD3 axis represents a promising therapeutic strategy for patients with DN. These results reveal AA targeting AMPD3 alleviates DN through ferroptosis in renal tubular epithelial by mitochondrial fragmentation in model of DN by HSP90a/Drp1 axis.

Keywords: histone lactylation; ferroptosis; AMPD3; METTL3; YTHDC1; diabetic nephropathy

Abbreviations

DN, diabetic nephropathy;

m6A, N6-methyladenosine;

METTL, methyltransferase;

CKD, chronic kidney disease;

ROS, reactive oxygen species;

AMPD, Adenosine monophosphate deaminase;

AMP, adenosine monophosphate;

AA, abietic acid;

HFD, high-fat die;

qPCR, quantitative polymerase chain reaction；

RIP, RNA immunoprecipitation;

GEO, Gene Expression Omnibus;

PAS, periodic acid-Schiff;

HE, hematoxylin and eosin

Cre, urinary creatinine, blood urea nitrogen (Bun), and 24 h urinary microalbuminuria

Bun, blood urea nitrogen;

mAlb, 24 h urinary microalbuminuria

MDA, malondialdehyde;

SOD, superoxide dismutase

GSH-PX, glutathione peroxidase;

GSH, Glutathione;

MCT, Monocarboxylic acid transporters;

GPR81, G protein-coupled receptor 81;

RMSD, Root Mean Square Deviation;

Rg, gyration;

SASA, solvent-accessible surface area;

RMSF, Root Mean Square Fluctuation;

SPR, surface plasmon resonance.

Introduction

With the development of society, the incidence rate of diabetes has been increasing year by year (1). Approximately 40% of diabetic patients will develop diabetic nephropathy, and among these individuals, 25% to 45% will progress to end-stage renal disease within the next 15 years (2). ESRD has a high mortality rate and poor prognosis. Early diagnosis and aggressive treatment can reverse diabetic nephropathy (DN) (3). Currently, commonly used clinical monitoring methods for DN include urine routine examination, urine microalbumin determination, glomerular filtration rate determination, and serum creatinine determination, but each method has certain limitations (4, 5). Therefore, finding indicators that reflect DN is crucial for early prediction of its occurrence and improving prognosis. The triglyceride-glucose index is calculated jointly from fasting blood glucose and fasting triglyceride (TG) values, which has high sensitivity and specificity for diagnosing insulin resistance (IR), is easy to obtain, and has attracted attention in clinical practice (6).

Epigenetic modification refers to heritable changes in gene expression levels and functions without altering the nucleotide sequence, including DNA methylation, histone post-translational modification, and non-coding RNA (ncRNA) (7). Epigenetic changes lead to the formation of high-glucose "metabolic memory" in target cells, resulting in complications such as DN, and ferroptosis is a core event in the progression of DN (8). Diabetes, as an independent risk factor for DN, makes exploring the mechanism of glucose metabolism in DN particularly important (9). Lactate is a central link in glucose metabolism and oxidative phosphorylation (10). Recently, lactate has been found to serve as a substrate for post-translational modification, which has a significant impact on protein function, but its role in DN has not been explored.

Glycometabolism is the primary pathway of cellular energy metabolism, and lactic acid, a product of glycolysis, was once considered a harmful metabolic waste under hypoxic conditions (10). Lactic acid can be produced and utilized under aerobic conditions, serving as an energy source for mitochondrial respiration, a substrate for

gluconeogenesis, and participating in lipid metabolism regulation. It can also function as a signaling molecule in cell signaling transduction. Lactylation modification sites have been identified in human and mouse cells, confirming the presence of lactylation modification on core histones, which plays a role in gene transcription regulation (11). Protein lactylation modification is widely present in cells (12). As a novel epigenetic modification using lactic acid as a substrate, lactylation modification participates in the regulation of various biological activities and plays an important role in the occurrence of diseases such as oxidative stress/inflammatory response (13). Lactylation modification of histones and non-histones can promote various biological activities by regulating the expression and function of METTL3 (14).

Among the up to 170 chemical modifications at the RNA transcriptome level that have been reported so far, N6-methyladenosine (m6A) stands out as the most prevalent post-transcriptional modification of mRNA in mammals (15). Reversible m6A modification plays a crucial role in mRNA splicing, stability, localization, and translation (16). Recent studies have revealed the role of methyltransferase (METTL)3, which is significantly upregulated in various kidney disease models, as well as in human kidney biopsies and cultured renal tubular epithelial cells (17-19). Furthermore, it has been found that silencing METTL3 can effectively alleviate renal tubular epithelial cell damage (20). This suggests that m6A RNA methylation modification is closely associated with the occurrence and development of DN (21).

The occurrence of diabetic nephropathy cannot be separated from the pathogenic role of IR (22). IR is closely related to early metabolic abnormalities and adverse cardiovascular outcomes in chronic kidney disease (CKD) (23). At the same time, CKD undergoes a series of pathophysiological changes, including inflammation, enhanced activity of the renin-angiotensin system, accumulation of uremic toxins, and metabolic acidosis (23). Research shows that ferroptosis participates in the occurrence and development of DN (24, 25). Ferroptosis is a newly discovered unique iron-dependent cell death mode, which is different from apoptosis, necrosis, and autophagy. This unique cell death mode is driven by lipid peroxidation catalyzed by free Fe2+ in the Fenton reaction, leading to the accumulation of reactive oxygen

species (ROS) in cells, ultimately causing membrane oxidative damage and inducing cell death (26). Ferroptosis is tightly regulated by multiple cellular metabolic pathways (iron metabolism, glucose metabolism, lipid metabolism, amino acid metabolism, etc.) and disease-related signaling pathways, and is involved in the occurrence and development of various diseases such as cardiovascular disease, brain disease, intestinal disease, liver disease, and cancer (27).

Adenosine monophosphate deaminase (AMPD) is a key enzyme that regulates energy metabolism dependent on adenosine monophosphate (AMP), playing an important role in cellular metabolism (28). AMPD is the central enzyme of energy metabolism in eukaryotes, capable of catalyzing the hydrolysis of adenosine monophosphate (AMP) to form inosine monophosphate (IMP) and ammonium ions ($NH4^+$), which plays a crucial role in the interconversion of purine nucleotides and energy metabolism (29). In muscle cells, the hypoglycemic drug metformin activates AMPK activity by inhibiting AMPD activity, thereby promoting glucose transport and fatty acid oxidation (30). Insulin resistance is one of the hallmark manifestations of obesity and type 2 diabetes (30). The AMPD3 gene is selectively highly expressed in skeletal muscle, which is one of the main organs where insulin resistance occurs (31). AMPD has a certain regulatory effect on insulin (32). In mice fed with high-fat diets, disruption of the AMPD3 gene leads to a reduction in the severity of insulin resistance, improved glucose tolerance, and enhanced insulin clearance (33).

Terpenoids are natural products characterized by novel, diverse molecular structures and broad biological activities, serving as crucial structural scaffolds for drug discovery and development (34). Notable examples include vinca alkaloids, paclitaxel, and camptothecin, which are all first-line chemotherapeutic agents in clinical use (35). Rosin is a highly significant natural resource often hailed as "petroleum growing on trees." It consists of various tricyclic diterpene resin acids—such as abietane-, pimarane-, and labdane-type resin acids—with abietic acid (AA) being the principal tricyclic diterpenoid component (36). Tricyclic diterpenoids like abietic acid possess novel and diverse structures coupled with relatively low molecular weights, suggesting the potential for improved bioavailability (37).

Although research on active rosin components, including AA, has primarily focused on industrial applications, their wide-ranging biological activities—such as antitumor, antibacterial, and antiviral properties—have been well-documented (38).

With the development of society, the incidence rate of DN has been increasing year by year. However, the underlying mechanisms of lactate's involvement in DN remain unclear. This study attempts to reveal the role and mechanism of Histone lactylation-regulated m6A-methylase on AMPD3 in DN.

Materials and Methods

Ethnic statements and patients

Blood samples were collected from healthy volunteers (n = 6) and DN patients (n = 20) according to the study protocol (2025-93) approved by the Ethics Committee of Yijishan Hospital of Wannan Medical College. We ensured that all participants or their relatives provided written informed consent. Peripheral venous blood (5-10 ml) was collected from DN patients.

Animal experiments

All C57BL/6 mice (5–6 weeks, 18–20 g) were randomly assigned to five groups: sham group (n = 8), model group (n = 8), Low/ Med/High CA group (n = 8), ME group (n = 8). DN mice were fed with a high-fat diet (HFD) for 12 weeks, and then injected with STZ (30 mg/kg of streptozotocin; Sigma-Aldrich, St Louis, MO, USA) i.p. for 7 consecutive days. Blood glucose levels were measured using 16.7 mmol/l after one week of the final injection. Low/Med/High AA (HY-N6871, MedChemExpress) group were administration with 20, 40 or 80 mg/kg/three days (dissolve in 4% ethanol solution in normal salina, i.p.) for 6 weeks as literature. Mice were killed under anesthesia, and kidneys and serum taken for analysis. This study was approved by the Animal Care and Use Committee of Yijishan Hospital of Wannan Medical College (WNWC-AWE-2025173).

Kidney tissue samples were fixed in 4% paraformaldehyde, paraffn-embedded and then sectioned into 5 μM slices for HE, Masson staining, PAS staining. Kidney tissue samples were observed using fluorescence microscope (Zeiss Axio Observer A1, Germany).

Vitro model and treatment with AA

Rat renal tubular epithelial (NRK-52E, Cell Bank of Chinese Academy of Sciences) cells were seeded in culture dish with RPMI 1640 (Gibco) supplemented with 10% FBS (Gibco) under a humidified 5% (v/v) CO2 atmosphere at 37°C. NRK-52E stimulated with 20 mmol/L d-glucose for 24-48 h. Next, the transfections were performed using Lipofectamine 2000 (Thermo Fisher Scientific). After 48 h of transfection, NRK-52E stimulated with 20 mmol/L d-glucose and Low/Med/High AA (20, 40 and 80 μmol/l) as literature (19).

Intracellular ATP level measurement, Determination of lipid peroxidation

Intracellular ATP levels were measured using an ATP assay kit (Beyotime, S0026) according to the manufacturer's instructions. NRK-52E cells were seeded in 6-well plates. The next day, the medium was replaced with fresh medium containing 20 mmol/L D-glucose for 24 h, and 10 mM L-lactic acid or PBS was added, respectively. After 12 h, the medium was discarded, and the cells were washed three times with PBS. Then, 200 μL of lysis buffer was added to each well to ensure complete cell lysis. Following centrifugation at 12,000g for 5 min at 4°C, the supernatant was collected and quantified using a microplate reader.

NRK-52E cells were seeded onto coverslips in 24-well plates. The following day, cells were stimulated with 20 mmol/L D-glucose for 24 h, followed by replacement with fresh medium containing 10 nM lactate for an additional 12 h. After discarding the medium, cells were washed three times with PBS. Subsequently, 10 μM C11-BODIPY581/591 (ThermoFisher, D3861) was added, and the cells were incubated in the dark for 30 min. Following three additional PBS washes, the cells

were examined and imaged using a fluorescence microscope.

ELISA, cell viability assay and quantitative polymerase chain reaction (qPCR)

ELISA was performed as described in a previous study (19). Cell viability was determined using CCK-8 assay as described in a previous study. Absorbance was measured on the Synergy H1 Microplate Reader (Bio Tek, Winooski). qPCR were performed with the ABI Prism 7500 sequence detection system according to the Prime-ScriptTM RT detection kit. Relative levels of the sample mRNA expression were calculated and expressed as $2^{-\triangle\triangle Ct}$.

Histological, immunohistochemical, and immunofluorescence analyses and electron microscopy

For immunohistochemical and immunofluorescence analyses, mouse lung tissue samples were fixed in 4% paraformaldehyde and stained with hematoxylin and eosin (HE) as described in previous study (19). Tissue samples were observed under a fluorescence microscope (Zeiss Axio Observer A1, Germany) and a transmission electron microscope (80 kV) (Hitachi H7650, Tokyo, Japan) as described in a previous study (19, 39).

Western Blotting Analysis and Immunofluorescence

Western Blotting Analysis were executed as literature (19). Protein was measured using an enhanced chemiluminescence system and analyzed using an Image Lab 3.0 (BioRad Laboratories, Inc.). For details of antibodies, with anti-AMPD3 Rabbit pAb (A6354, abclonal, 1:1000), anti-METTL3 antibody (AB195352, abcam, 1:1000), anti-METTL14 antibody (AB220030, abcam, 1:1000), anti-YTHDC1 antibody (ab122340, abcam, 1:1000), anti-GPCR GPR81 antibody (ab106942, abcam, 1:1000), anti-GAP43 Rabbit mAb (A19055, abclonal, 1:1000), anti-Hsp90α/β Rabbit mAb (A5027, abclonal, 1:1000), anti-Phospho-DRP1-S616 Rabbit mAb (AP1573, abclonal, 1:1000), anti-MCU Rabbit mAb (A22525, abclonal, 1:1000), β-Actin (BS6007MH, Bioworld Technology, Inc., 1:5000).

Immunofluorescence and electron microscope

Electron microscopes were executed as described previously (19). Cells were incubated with anti-AMPD3 Rabbit pAb (A6354, abclonal, 1:1000), anti-METTL3 antibody (AB195352, abcam, 1:1000), anti-METTL14 antibody (AB220030, abcam, 1:1000), anti-YTHDC1 antibody (ab122340, abcam, 1:1000), anti-GPCR GPR81 antibody (ab106942, abcam, 1:1000), anti-GAP43 Rabbit mAb (A19055, abclonal, 1:1000), anti-Hsp90α/β Rabbit mAb (A5027, abclonal, 1:1000), anti-Phospho-DRP1-S616 Rabbit mAb (AP1573, abclonal, 1:1000), anti-MCU Rabbit mAb (A22525, abclonal, 1:1000) at 4°C overnight after blocking with PBS supplemented with 5% BSA for 2 h at room temperature. Cell samples were observed using fluorescence microscope (Zeiss Axio Observer A1, Germany). Ultra-thin sections were observed using a Hitachi H7650 transmission electron microscope (Tokyo, Japan).

Microscale thermophoresis (MST), thermal shift assay (TSA), and cellular thermal shift assay (CETSA)

MST, TSA and CETSA were executed as described previously. 0.10 mg/mL WT AMPD3 protein was used with or without 0.50 mmol/L AA in PBS. 20 μL supernatant was used to Western blotting. CETSA, and the thermal stability were performed using GraphPad Prism software (GraphPad Diego, CA, USA).

Single Cell Analysis

Cell barcode filtering, alignment, and UMI counting were performed using gastric cancer and influenza patients. The tissue-specific expression of AMPD3 in patients with DN was evaluated using single-cell data from the China National GeneBank and the GSE195460 dataset from Gene Expression Omnibus (GEO). The cancer tissue sample was from a DN patient with untreated, primary, nonmetastatic gastric tumor who underwent DN resection.

Molecular docking model

Complexes were color-labeled, and 3D surface display was utilized according to the previously described (Zhang et al., 2025). AMPD3 (2A3L), HSP90a (7lsz) protein structures were obtained from RCSB PDB. Protein interaction analysis identified AMPD3 binding regions on HSP90a, and imported into Pymol (version 2.3.0) to remove water molecules and small molecules.

Bioluminescence imaging

cHS4I-hAMPD3-Luc transgene transgenic mice were structured according to the previously described (Zhang et al., 2025). Bioluminescent imaging was performed using an IVIS imaging system (Bio-Real, QuickView3000, Austria).

qChIP, Global m6A measurement and m6A dot blot assay

Based on the manufacturer's instructions, the ChIP assay was performed using the Simple ChIP Plus Sonication Chromatin IP Kit from Cell Signaling Technology (Cat# 9003). In brief, NRK-52E cells were cross-linked with 1% formaldehyde, and chromatin was sheared into 200–300 bp fragments using a Bioruptor Pico. The fragmented chromatin was then immunoprecipitated overnight at 4°C with either H3K14la antibody or normal IgG (negative control). The next day, immune complexes were captured using protein A/G magnetic beads, followed by elution, reversal of cross-links, and DNA purification. Finally, the enriched DNA was quantified by qChIP using ChamQ Universal SYBR qPCR Master Mix.

Colorimetric quantification of m6A levels in total RNA was performed using the m6A RNA Methylation Quantification Kit (Epigentek, Cat# P-9005-96), where 200 ng of RNA was coated per well and concentrations were calculated from a standard curve. Total RNA was extracted and mRNA was purified, denatured at 95°C, and spotted onto Amersham Hybond-N+ membranes. Following UV cross-linking, the membranes were incubated with an anti-m6A antibody (1:1000, Synaptic Systems, Cat# 202003) overnight at 4°C, washed, and then incubated with a secondary antibody. Detection was carried out using an ECL chemiluminescence kit (Tanon, Cat# 180–

5001); simultaneously, membranes were stained with methylene blue as a loading control.

MeRIP-qPCR, RNA immunoprecipitation (RIP) q-PCR and Assessment of mRNA stability

Based on the manufacturer's instructions, MeRIP was performed using the EpiQuik CUT&RUN m6A RNA Enrichment Kit (Epigentek, Cat# P-9018-24). Briefly, cell lysates were incubated with m6A antibody-conjugated magnetic beads at room temperature for 2 h, followed by proteinase K digestion. RNA bound to the antibody-bead complexes was then extracted using a phenol-chloroform-isoamyl alcohol mixture. The enrichment of m6A-modified RNA was analyzed by real-time quantitative RT-PCR. Additionally, the SRAMP online tool was used to predict m6A sites within AMPD3 for primer design.

Based on the manufacturer's protocol (BerSinBio# Bes5101), we performed RNA Immunoprecipitation (RIP) to investigate the interaction between YTHDC1 protein and AMPD3 mRNA. Briefly, cells were washed with PBS, lysed, and treated to remove DNA. The resulting lysate was divided into three groups: input, IP, and IgG control. The IP and IgG groups were incubated overnight at 4°C with YTHDC1 antibody or IgG antibody, respectively, followed by incubation with protein A/G magnetic beads to isolate RNA-protein complexes. After proteinase K digestion and RNA extraction, the relative abundance of the immunoprecipitated RNA was analyzed by qRT-PCR.

Alveolar epithelial cells from different groups were treated with actinomycin D (Sigma-Aldrich, A9415) for 0, 2, 4, and 6 h, respectively. Total RNA was extracted from NRK-52E cells using TRIzol reagent (Takara) and analyzed by qPCR. The mRNA half-life was subsequently estimated using linear regression analysis.

Statistical Analysis

$P < 0.05$ was considered significant and evaluated using Student’s t-test or one-way analysis of variance (ANOVA) followed by Tukey’s post-test. Data were expressed as

mean ± standard deviation (SD).

Results

Inhibition of lactate alleviates Diabetic nephropathy

The experiment determined the expression and effects of lactate in patients with DN, serum lactate in patients with DN was increased (Figure 1A). Meanwhile, serum lactate is positively correlated with BUN, CRE, and mAlb in patients with DN (Figure 1B-1D). However, there was negative correlation between lactate and GSH in patients with DN (Figure 1E).

Next, in mice model of DN, serum lactate was also increased (Figure 1F). Applying these two inhibitors, 2-DG and oxamate, DN mice was injected with 2-DG or oxamate to reduce circulating lactate levels in mice (Figure 1G-1H). 2-DG or oxamate reduced BUN, CRE, and mAlb in DN mice (Figure 1I-1K). 2-DG or oxamate also improved glomerular structural damage and renal fibrosis in DN mice (Figure 1L). 2-DG or oxamate also increased SOD, GSH-PX and GSH activity levels, and reduced MDA levels in DN mice (Figure 1M-1P). The above results suggest that inhibition of lactate can effectively attenuate oxidative stress and improve renal function and structure in DN mice.

Lactate induces H3K14la increase in DN

Since lactate is widely recognized as the essential substrate for lactylation, it is reasonable to postulate that lactylation levels are modulated in the context of DN. Next, an increase in pan-lysine lactylation (pan-Kla) protein and mRNA levels in the kidney tissue of DN mice (Figure 2A-2B). We found that histone H3 lysine 14 lactylation (H3K14la) was markedly elevated in the renal tissues of DN mice relative to the sham-operated group (Figure 2C–2E). Consistent with this finding, immunofluorescence assays further confirmed enhanced H3K14la abundance in the kidneys of DN mice (Fig. 2F). In the in vitro DN model, treatment with lactate significantly up-regulated both the mRNA and protein expression levels of pan-lysine

lactylation (pan-Kla) and H3K14la (Figure 2G–2H). Collectively, these results verify that the high-lactate microenvironment induced by DN promotes the upregulation of H3K14la in murine renal tissues.

Lactate/H3K14la axis increase m6A modification by METTL3

N6-methyladenosine (m6A) modification, a pivotal epigenetic regulatory mechanism, exerts critical modulatory effects on the pathogenesis of tumors, inflammatory disorders, and autoimmune diseases. To elucidate the alterations in RNA m6A modification associated with DN, we quantified the abundance of m6A-methylated RNA in renal tissues derived from mice subjected to high-glucose induction and their corresponding control counterparts.

In patients with DN, Lactate levels were positively correlated with METTL3 expression; meanwhile, lactate was also positively correlated with YTHDC1, but showed no correlation with METTL14, YTHDF1, YTHDF2 or YTHDC2 (Figure 3A-3F). In DN mice model, our results revealed a significant upregulation of m6A in the kidney tissue of DN mice (Figure 3G-3H). Our findings revealed a significant up-regulation of METTL3 and YTHDC1 expression after 12 h of lactate treatment among all methyltransferases (Figure 3I). Of course, lactate increased METTL3 and YTHDC1 protein expression levels in vitro model of DN (Figure 3J-3K).

To further verify the role of GPR81 signaling, we employed GPR81 siRNA to knockdown GPR81 expression. Consistent with our previous findings, lactate-induced METTL3 activation was suppressed upon GPR81 downregulation (Figure 3L). Meanwhile, in our in vitro model, lactate markedly enhanced the enrichment of H3K14la at the METTL3 locus (Figure 3M). Collectively, our results demonstrate that m6A modification levels are elevated in DN, and lactate plays a critical role in mediating this process (Figure 3N).

GPR81/METTL3/YTHDC1 axis mediates AMPD3 mRNA stability through m6A modification by METTL3

This study explored the disease targets for the occurrence and progression of DN.

AMPD3 expression was in DN samples (GSE154881) were up-regulated (Figure 4A). Then, AMPD3 mRNA expression was up-regulated in patients with DN (Figure 4B). AMPD3 protein and mRNA expression levels were increased in mice with DN (Figure 4C-4D). Immunohistochemistry also showed that AMPD3 expression was also increased in renal tissue of mice with DN (Figure 4E-4F).

Next, this experiment showed that lactate stimulation promotes the upregulation of AMPD3 mRNA and protein expression, with the most significant upregulation observed 6 h after lactate stimulation in vitro model of DN (Figure 5A). AMPD3 possesses multiple suspected methylation modification sites in proximity (Figure 5B).Me-RIP analysis demonstrated that lactate upregulated the m6A enrichment of AMPD3 (Figure 5C). However, METTL3 knockdown using sh-METTL3 significantly inhibited lactate-induced m6A enrichment (Figure 5C). We examined AMPD3 mRNA and protein levels in response to lactate stimulation (Figure 5D). METTL3 knockdown or si-YTHDC1 reduced AMPD3 mRNA and protein level (Figure 5D).

We further assessed the stability of AMPD3 after lactate stimulation in the presence of si-NC, si-METTL3, and si-YTHDC1. By measuring the mRNA levels of AMPD3 after Actinomycin D treatment using qPCR, we found that the enhanced stability and increased half-life of AMPD3 induced by lactate were suppressed after knocking down METTL3 or YTHDC1 (Figure 5E-5F).

Additionally, we examined the impact of METTL3 and YTHDC1 on lactate-induced ferroptosis in NRK-52E cells. When si-RNA was transfected to knock down METTL3 and YTHDC1, the downregulation of GPX4 protein expression induced by lactate in NRK-52E cells was reversed (Figure 5G-5H). Moreover, the knockdown of METTL3 and YTHDC1 attenuated the suppression of cell viability caused by lactate (Fig. 5K and L). Collectively, these findings shed light on the role of METTL3 in promoting AMPD3 mRNA m6A modification and stabilizing AMPD3 through a YTHDC1-dependent pathway, thus exacerbating lactate-induced ferroptosis in

pulmonary epithelial cells in model of DN.

Monocarboxylic acid transporters (MCT) and G protein-coupled receptor 81 (GPR81) are common receptors contributing as lactate receptors. We treated NRK-52E cells with the MCT inhibitor [2-cyano-3-(4-hydroxyphenyl)-2-propenoic acid (CHCA)] and examined the expression of METTL3 was down-regulation and GPX4 protein expression was induced (Figure 5K). These results suggest that MCT1, as a lactate transporter, plays a role in regulating METTL3 and downstream signals.

We then pre-treated NRK-52E with the GPR81 antagonist 3-hydroxy butyrate acid (3-OBA) before lactate stimulation and found that 3-OBA suppressed the lactate-induced up-regulation of METTL3 and AMPD3 expression while restoring lactate-induced changes in ferroptosis signalling (Figure 5L).

When GPR81 was down-regulated, lactate-induced METTL3/ AMPD3 activation and ferroptosis were suppressed in vitro model of DN (Figure 5M). When si-MCT1 and si-GPR81 are combined, the most significant inhibition of lactate-induced ferroptosis signalling occurs (Figure 5N).

Collectively, our results showed that lactate-activated AMPD3 expression via activation of METTL3 upregulation by GPR81 signalling promotes ferroptosis in model of DN.

This study delved into the specific cell types of AMPD3 in the model of DN through Single Cell Analysis (Figure 6A). Subsequently, the expression of AMPD3 in DN patients was assessed using Single Cell Analysis (Figure 6A). AMPD3 was expressed in renal tubular epithelial in DN patients (Figure 6B). AMPD3 was not found to be expressed in B cells, T cells and macrophage of DN patients (Figure 6C-6E). So, GPR81/METTL3/YTHDC1 axis induced AMPD3 mRNA stability through m6A modification by METTL3.

METTL3-mediated AMPD3 induces ferroptosis via mitochondrial fragmentation

There is evidence suggesting that mitochondria play a crucial role in ferroptosis in

model of DN. Lactate stimulation in mitochondrial morphology at 6 h, there was no significant change after 6 h of stimulation (Figure 7A). We further investigated the changes in ATP levels and mitochondrial-related mRNA expression in NRK-52E cells over time after lactate treatment. Interestingly, we found that ATP levels, mitochondrial membrane potential (MMP) and mitochondrial-related mRNA were upregulated in the early stages (1, 3, and 6 h) of lactate stimulation, whereas they decreased as lactate stimulation time extended (Figure 7B-7E). Meanwhile, we also found that there was no significant change in cellular glycolysis level (Figure 7F-7G). Lactate stimulation reduced mitochondria CoCl2 levels and JC-1 assay levels, and increased iron concentration levels in vitro model of DN (Figure 7F-7I).

We speculated that lactate stimulation-induced mitochondrial activation and ROS accumulation are mediated by via the Drp1 pathway (Figure 7J). Lactate stimulation induced AMPD3, HSP90a, p-Drp1, Mcu protein expression levels in vitro model of DN (Figure 7K).

To clarify whether lactate-induced changes in mitochondrial metabolism depend on AMPD3 by METTL3, we knocked down METTL3 in NRK-52E cells using lentiviral vectors. The results show that the upregulation of mitochondrial-related mRNA induced by lactate stimulation for 6 h was restored after METTL3 downregulation (Figure 7L). Additionally, the upregulation of AMPD3, HSP90a, p-Drp1 induced by lactate was suppressed in the sh-METTL3 group, the down-regulation of GPX4 reduced by lactate was also induced in the sh-METTL3 group (Figure 7M). Meanwhile, the down-regulation of mitochondria CoCl2 levels and JC-1 assay levels, and the up-regulation of iron concentration levels induced by lactate was reduced in the sh-METTL3 group (Figure 7N-7P). sh-METTL3 could reduce mitochondrial damage by lactate in vitro model of DN (Figure 7Q).

Meanwhile, we found that sh-METTL3 effectively improved the increase in lipid peroxidation induced by lactate (Figure 7R). Herein, we revealed that lactate-induced transient enhancement of mitochondrial activity is mediated by the involvement of METTL3 and AMPD3. Moreover, we provide evidence for the crucial role of METTL3-mediated AMPD3 in lactate-induced ROS accumulation and lipid

peroxidation induces ferroptosis via mitochondrial fragmentation.

AMPD3 induced HSP90a/Drp1 to promote mitochondrial fragmentation by MCU

This study elucidated that the function and mechanism of AMPD3 on ferroptosis in model of DN. Treatment with sh- AMPD3 virus significantly reduced renal injury (Renal sinus injury), as evidenced by decreased kidney-to-body weight ratio and water intake (Figure 8A-8B). Sh-AMPD3 decreased urinary albumin excretion, serum creatinine levels and urinary nitrogen in a mouse model of DN (Figure 8C-8E). Next, sh-AMPD3 increased E-cadherin mRNA, and reduced periostin mRNA levels in renal tissue (Figure 8F-8G). Sh-AMPD3 also reduced MDA level, and increased SOD, GSH and GSH-PX levels in mice model of DN (Figure 3H-3K). Sh-AMPD3 reduced Ferrous iron levels, suppressed AMPD3, HSP90a, p-Drp1 protein expression levels, and induced GPX4 protein expression levels in mice model of DN (Figure 8L-8M). Sh-AMPD3 exacerbated kidney damage in mice model of DN (Figure 8N).

In vitro model of DN, AMPD3 up-regulation induced AMPD3, HSP90a, p-Drp1 protein expression levels, and suppressed GPX4 protein expression levels (Figure 8O). AMPD3 up-regulation reduced GSH level and JC-1 assay levels, increased MDA level and iron concentration levels in vitro model of DN (Figure 8O-8S). This trend is reversed by si-AMPD3 in vitro model of DN (Figure 8T-8X). Herein, AMPD3 induced HSP90a/Drp1 to promote mitochondrial fragmentation by MCU

AMPD3 interacted with HSP90a by promoting its K63-linked polyubiquitination and proteasomal degradation

Next, this study elucidated that the mechanism of AMPD3 on HSP90a in model of DN. In an in vitro model of DN, immunofluorescence showed that AMPD3 up-regulation induced AMPD3 and HSP90a expression (Figure 9A). In mice model of DN, immunofluorescence showed that sh-AMPD3 suppressed AMPD3 and HSP90a expression in renal tissues of DN mice model (Figure 9B). IP assay showed that lactate stimulation increased the AMPD3 protein interacts with HSP90a protein in vitro model od DN (Figure 9C).

As shown in Figure 9D, K63-only Ub, but not K48-only Ub, enabled the polyubiquitination of HSP90a similar to WT Ub. The finding suggests that the AMPD3-catalyzed poly Ub modification of HSP90a is primarily dependent on the presence of the K63-linkage. Furthermore, AMPD3 mediated K63-linked polyubiquitination of HSP90a was significantly enhanced by proteasome inhibitor MG132 but not lysosome inhibitor CQ (Figure 9E). Consistently, AMPD3-mediated degradation of HSP90a was considerably hindered by MG132 rather than CQ (Figure 9E).

3D model prediction and found that the AMPD3 protein interacts with the HSP90a protein (Figure 9F-9G). IP analysis demonstrated that AMPD3 WT protein interacts with the HSP90a WT protein, while the AMPD3 WT protein does not interact with the HSP90a Mut protein, and the HSP90a Mut protein does not link with the AMPD3 WT protein (Figure 9H), suggesting AMPD3-induced degradation of HSP90a through proteasome pathway.

Screening of potential compounds that can target AMPD3

According to the above results, histone lactylation-regulated m^{6}A-methylase METTL3 accelerates AMPD3-mediated ferroptosis in diabetic nephropathy. We aim to identify and screen compounds that can effectively bind to AMPD3 as an important strategy for the treatment of DN (Figure 10A). We found that abietic acid (AA) exhibited a good binding rate to AMPD3 (Figure 10B).

From this, AA was identified AMPD3 as a candidate. It demonstrated binding to AMPD3 at the 402H, 502L, 508E, 540N, 574L, 747P and 748L (Figure 10C). Meanwhile, AA could not regulated AMPD3 mRNA expression, and this result excludes the regulation of the AMPD3 gene expression levels by AA (Figure 10D). Subsequent Cellular Thermal Shift Assay (CETSA) results confirmed that AA acid specifically stabilized the wild-type (WT) AMPD3, but not the mutant (Mut) form, against thermal denaturation (Figure 10E). AA increased the protein's melting temperature from ~55°C to ~67°C (Figure 10F-10H). AA promoted AMPD3 protein expression ubiquitination in vitro model (Figure 10I). These results provide

conclusive evidence that AA directly binds to AMPD3, forming the mechanistic basis for its use in model DN.

The Root Mean Square Deviation (RMSD) of the complex structure gradually stabilized over the course of the simulation, demonstrating that the complex conformation reached a steady state. Additionally, the gradual stabilization of the radius of gyration (Rg), as illustrated in the figure, further confirmed the increasing stability of the complex formed by the ligand and receptor protein. The buried solvent-accessible surface area (SASA) increased steadily during the simulation, eventually converging with diminishing fluctuations, which suggests that the contact area and binding interface between the receptor and ligand proteins gradually stabilized, reflecting a progressively more stable interaction. Root Mean Square Fluctuation (RMSF) is indicative of the flexibility of amino acid residues in a protein, with higher RMSF values corresponding to greater residue flexibility (Figure 10J).

We evaluated the binding of AA to recombinant human AMPD3 proteins using surface plasmon resonance (SPR) assays. As shown in Figure 10K, SPR assays revealed that AA exhibited the strongest binding affinity for AMPD3. So, AA directly binds to AMPD3 protein in model of DN.

AA Targeting AMPD3 alleviates DN through ferroptosis by mitochondrial fragmentation

Next, this study elucidated that the effect of AA Targeting AMPD3 alleviates DN. AA suppressed the protein expression of AMPD3/ HSP90a/p-Drp1, and induced GXP4 protein expression in renal tissues of DN mice model (Figure 11A). AA improved glomerular structural damage and renal fibrosis in DN mice (Figure 11B). AA reduced kidney-to-body weight ratio and water intake, decreased urea nitrogen, MDA level, improved GSH levels in renal tissues of DN mice model (Figure 11C-11G). AA also suppressed the protein expression of AMPD3/ HSP90a/p-Drp1, and induced GXP4 protein expression in vitro model of DN (Figure 11H). AA reduced MDA levels and iron concentration levels, and increased GSH levels in vitro model of DN (Figure 11I-11K). Therefore, AA targeting AMPD3 alleviates DN through ferroptosis by

mitochondrial fragmentation.

AA reduced the interaction between the interconnection of AMPD3 and HIF1α

To further confirm these findings, we synthesized Biotin-AA conjugates, and found that Biotin- AA specifically pulled down AMPD3 in biotin-pull down assays (Figure 12A). The addition of free AA in cells significantly inhibited the binding of Biotin-AA to AMPD3 (Figure 12B). Moreover, the binding of Biotin- AA with AMPD3 was dose-dependent (Figure 12C). Additionally, Biotin- AA and FASN were colocalized in the NRK-52E cells (Figure 12D). These results collectively demonstrate a specific and direct binding between AA and the AMPD3 protein, supporting the potential of AA as a targeted agent against AMPD3.

Discovery of live imaging, AA is concentrated in kidney tissue (Figure 12E). Meanwhile, AA suppressed the AMPD3 expression in kidney of DN mice model (Figure 12F). Therefore, AA combined AMPD3 protein in macrophage in kidney of DN model.

The co-immunoprecipitation assay confirmed that AA decreased the interaction between the interconnected AMPD3 and HIF1αin NRK-52E cells treated with high glucose (Figure 12G). These findings imply that AA reduces the interaction between the interconnected FASN and HIF1α.

Discussion

China is one of the countries with the highest number of diabetes patients, with a prevalence rate of about 10.9%, and approximately 114 million diabetes patients, of which 30% to 40% will develop diabetic nephropathy (40). Diabetic nephropathy is one of the most common and severe complications of diabetes, leading to health problems such as renal failure, cardiovascular diseases, hypertension, anemia, osteoporosis, etc (41). Hyperlipidemia is a risk factor for diabetic nephropathy. Abnormal blood lipids lead to lipid deposition in blood vessels, formation of plaques, and other factors that cause vascular hardening, which is the pathological basis for the occurrence and development of diabetic nephropathy (42). In addition, abnormal

blood lipids may also affect diabetic nephropathy through mechanisms such as oxidative stress, inflammatory response, endothelial dysfunction, and thrombosis (43). Lactate can serve as a precursor for histone lysine lactylation, regulating the transcription of chromatin (44). It has been clearly established that both endogenous and exogenous lactate can elevate protein Kla levels (45). A recent study discovered a positive feedback loop involving glycolysis-lactate-H4K12 lactylation-activated glycolysis in renal cells of humans and mice with kidney disease (46, 47). In this study, the expression and effects of lactate in patients with DN, serum lactate in patients with DN was increased. Zheng et al. showed that Lactate triggered histone lactylation in DN model (48). Therefore, the inhibition of Lactate was a promising therapeutic compound for the treatment of DN or diabetes-related diseases.

Histone is the main protein component of chromatin and plays a crucial role in the regulation of biological genetic information (49). Lactic acid, a common product of cellular metabolism, can affect the expression of cellular genetic information. Under the action of relevant enzymes, histones undergo various chemical modifications of groups, among which lactic acidification is one of the important chemical modifications (50). Lactic acid, a product of cellular glycolysis, and related hydrogen ions are usually immunosuppressive negative factors, but they can enhance the functions of helper T cells, dendritic cells, natural killer (NK) cells, and neutrophils (51). Histone lactic acidification regulates physiological functions such as macrophage aggregation and infiltration, and regulates cellular ROS levels by regulating the expression of METTL-3 (14). We found that the inhibition of lactate alleviates DN. Hu et al. reported that Lactate triggers ferroptosis in diabetic nephropathy (52). Therefore, lactate can target ferroptosis in model of DN.

In recent years, research has found that the progression of DKD is associated with epigenetic mechanisms (49). Epigenetic mechanisms mainly include DNA methylation, histone modification, non-coding RNA, etc., which exacerbate processes such as GFR decline, renal fibrosis, and inflammatory response through molecular mechanisms such as gene methylation, histone ubiquitination, acetylation, and phosphorylation (53). DNA methylation is one of the most common forms of

epigenetic modifications, among which 6-methyladenosine (m6A) modification is catalyzed by methylation complexes, including methyltransferase 3, methyltransferase 14, and RNA methyltransferase complex, playing a crucial role in RNA processing, stability, and translation (54). In SI-AKI, the dysregulation of RNA methylation, particularly m6A, drives the pathological process of the kidney by altering mRNA stability, alternative splicing, and protein synthesis. m6A (including METTL3) may participate in the occurrence and development of vascular-related diseases by regulating cellular pathways, fibrosis, angiogenesis, inflammatory response, etc. METTL3-mediated n6-methyladenosine (m6A) modification is associated with many physiological and DN pathological processes (53). In this study, Lactate/H3K14la axis increase m6A modification by METTL3. GPR81/METTL3/YTHDC1 axis mediates AMPD3 mRNA stability through m6A modification by METTL3. Toshifumi Ogawa et al. revealed that AMPD3 insight into mechanisms contributing to the development of diabetic cardiomyopathy (55). So, we speculated that the inhibition of AMPD3 gene might effectively target Lactate/H3K14la-induced DN to exert effects against ferroptosis in model of DN by GPR81/METTL3/YTHDC1 axis.

The pathogenesis of diabetic nephropathy (DN) is quite complex. Ferroptosis, as a newly discovered cell death mode, has become a research hotspot in recent years, and DN is closely related to ferroptosis (56). Factors such as SystemXc--GSH-GPX4 axis inactivation, iron overload, lipid peroxidation, and mitochondrial dysfunction play an important role in the occurrence and development of ferroptosis in DN (57). Antioxidant proteins may be potential targets for the treatment of ferroptosis in DN (58). By activating antioxidant proteins such as GPX4, Nrf2, Sirtuin family proteins, and ferritin, the occurrence and development of ferroptosis can be alleviated through different pathways and interactions (59). This experiment showed that METTL3-mediated AMPD3 induces ferroptosis via mitochondrial fragmentation. Cheng et al. showed that AMPD3 promotes ferroptosis in model of doxorubicin-induced cardiomyopathy (32). Here, we found that the inhibition of AMPD3 gene exerted anti-mitochondrial damage effect, thus protecting against ferroptosis in model of DN.

Research has shown that excessive mitochondrial fission is involved in the pathogenesis of apoptosis in DN renal cells (60). The kinase anchor protein 1 (AKAP1)/dynamin-related protein 1 (Drp1) pathway is an important pathway for mitochondrial fission in podocytes of diabetic kidney disease (DKD) (61). AKAP1 can mediate the phosphorylation of Drp1 at Ser637, leading to the translocation of Drp1 to mitochondria and inducing mitochondrial fission and podocyte apoptosis (62). Therefore, inhibiting mitochondrial fission mediated by the Drp1 pathway, maintaining mitochondrial homeostasis, and reducing renal cell damage may be an effective means to delay the progression of DN (61). We found that AMPD3 induced HSP90a/Drp1 to promote mitochondrial fragmentation by MCU. Arata Osanami et al. suggest that AMPD3 induced mitochondrial Ca2+ overload in type 2 diabetes hearts (63). This study mainly focused on the inhibition of AMPD3 gene on ferroptosis in model of DN by the suppression of HSP90a/Drp1 signaling pathway.

Ca2+-induced mitochondrial calcium release is caused by the opening of Ca2+-induced mPTP, resulting in DN (64). Due to reperfusion, cells become filled with calcium, triggering the extensive opening of mPTP, which directly leads to large DN (65). ROS accumulates significantly and damages mitochondrial DNA and mitochondrial membranes, causing mitochondrial membrane rupture, releasing apoptosis factors such as cytochrome C, leading to cardiomyocyte apoptosis (66). The rapid accumulation of large amounts of ROS within mitochondria also causes irreversible rupture damage to mitochondria, resulting in DN (67). HSP90 further promotes mitophagy, strengthening and maintaining the dynamic homeostasis of mitochondria. HSP90 may have the function of regulating mitophagy by acting as a molecular chaperone for mitochondrial membrane surface-associated proteins. In this study, AMPD3 induced HSP90a/Drp1 to promote mitochondrial fragmentation by MCU. AMPD3 interacted with HSP90a by promoting its K63-linked polyubiquitination and proteasomal degradation. Cheng et al. showed that AMPD3 promotes ferroptosis in model of doxorubicin-induced cardiomyopathy by HSP90α/DRP1 (32).

Traditional Chinese medicine (TCM) is characterized by its multi-component,

multi-target, and multi-pathway holistic regulation (68). The active components of TCM and TCM formulas have potential application value in improving DN renal damage and ferroptosis by enhancing the expression of antioxidant proteins, providing new research directions for delaying the progression of DN (69, 70). Specifically, AA exhibits antitumor, antioxidant, and antidiabetic activities. In this study, AA Targeting AMPD3 alleviates DN through ferroptosis by mitochondrial fragmentation. Nur Ainina Abd Wahab et al. showed that AA ameliorates nephropathy progression in diabetic model (71). Collectively, these results verified that AA targeted the inhibition of AMPD3 gene for ferroptosis in model of DN by the suppression of HSP90a/Drp1 signaling pathway.

Our findings suggest that a histone lactylation induces ferroptosis via the GPR81/METTL3/YTHDC1/ AMPD3 axis in renal tubular epithelial during DN. Targeting METTL3/YTHDC1/ AMPD3 axis represents a promising therapeutic strategy for patients with DN (Figure 13). These results reveal AA targeting AMPD3 alleviates DN through ferroptosis in renal tubular epithelial by mitochondrial fragmentation in model of DN by HSP90a/Drp1 axis. This study uncovers a critical molecular mechanism in diabetic nephropathy (DN) progression, where histone lactylation induces ferroptosis in renal tubular epithelial cells via the GPR81/METTL3/YTHDC1 axis. Its significance lies in establishing AA targeting AMPD3 as a promising therapeutic strategy, which effectively alleviates ferroptosis and ameliorates DN by regulating HSP90a/Drp1-mediated mitochondrial fission

Declaration of Interest Statement

We wish to confirm that there are no known conflicts of interest associated with this publication and there has been no significant financial support for this work that could have influenced its outcome.

Authors' contribution

Qin Yin and Zhichen Pu conceived the study, designed the study and prepared the

manuscript. Weiwei Zhang, Meng Wang and Yinping Shui, conducted the experiments and data analysis, involved in preparation of the figures and manuscript. All data were generated in-house, and no paper mill was used. All authors agree to be accountable for all aspects of work ensuring integrity and accuracy.

Funding

This work was supported by Key Natural Science Projects of the Department of Education of Anhui province (2022AH051242, 2024AH051917, 2024AH051958, 2025AHGXZK31475); Wuhu Science and Technology Project (2025KJ059).

Data Availability of Statement

The datasets used and/or analyzed of this study are from corresponding author upon reasonable request.

Declaration of Interest Statement

We wish to confirm that there are no known conflicts of interest associated with this publication and there has been no significant financial support for this work that could have influenced its outcome.

Authors' contribution

Qin Yin and Zhichen Pu conceived the study, designed the study and prepared the manuscript. Weiwei Zhang, Meng Wang, Yinping Shui conducted the experiments and data analysis, involved in preparation of the figures and manuscript. All data were generated in-house, and no paper mill was used. All authors agree to be accountable for all aspects of work ensuring integrity and accuracy.

Funding

This work was supported by Key Natural Science Projects of the Department of

Education of Anhui province (2022AH051239, 2023AH051767, 2024AH051917, 2024AH051958); Talent Introduction Research Fund Project of Wannan Medical College (WK2023ZZD16, WK2024ZZD06); Wuhu Science and Technology Plan Project (2025KJ059); Hengrui Research Fund Cross disciplinary Project for School Enterprise Integration Development (XQHR202426).

Data Availability of Statement

The datasets used and/or analyzed of this study are from corresponding author upon reasonable request.

References

1. Li J, Zhuang Y, Fan G*, et al*: Impact of baicalin and components of Scutellaria baicalensis on renal fibrosis of diabetic kidney disease. Front Pharmacol 15: 1480626, 2024.

2. Liu M, Yang W, Qu S*, et al*: Loss of glomerular aldolase B in diabetic nephropathy promotes renal fibrosis via activating Akt/GSK/β-catenin axis. J Adv Res2024.

3. Li C, Geng C, Wang J*, et al*: Investigating the inflammatory mechanism of notoginsenoside R1 in Diabetic nephropathy via ITGB8 based on network pharmacology and experimental validation. Mol Med 30: 277, 2024.

4. Lv N, Jia L, Liu F*, et al*: Elevated circulating homocysteine concentrations delayed nerve conduction velocity and increase the risk of diabetic kidney disease in patients with type 2 diabetes. Front Endocrinol (Lausanne) 15: 1451758, 2024.

5. Zhang W, Liu Y, Zhou J, Qiu T, Xie H and Pu Z: Chicoric acid advanced PAQR3 ubiquitination to ameliorate ferroptosis in diabetes nephropathy through the relieving of the interaction between PAQR3 and P110α pathway. Clin Exp Hypertens 46: 2326021, 2024.

6. Karimi F, Moazamfard M, Taghvaeefar R, *et al*: Early Detection of Diabetic Nephropathy Based on Urinary and Serum Biomarkers: An Updated Systematic Review. Adv Biomed Res 13: 104, 2024.

7. Kato M and Natarajan R: Epigenetics and epigenomics in diabetic kidney disease and metabolic memory. Nat Rev Nephrol 15: 327-345, 2019.

8. Kushwaha K, Garg SS and Gupta J: Targeting epigenetic regulators for treating diabetic nephropathy. Biochimie 202: 146-158, 2022.

9. Li X, Lu L, Hou W, *et al*: Epigenetics in the pathogenesis of diabetic nephropathy. Acta Biochim Biophys Sin (Shanghai) 54: 163-172, 2022.

10. Chen L, Huang L, Gu Y, Cang W, Sun P and Xiang Y: Lactate-Lactylation Hands between Metabolic Reprogramming and Immunosuppression. Int J Mol Sci 232022.

11. Li W, Zhou C, Yu L, *et al*: Tumor-derived lactate promotes resistance to bevacizumab treatment by facilitating autophagy enhancer protein RUBCNL expression through histone H3 lysine 18 lactylation (H3K18la) in colorectal cancer. Autophagy 20: 114-130, 2024.

12. Fan H, Yang F, Xiao Z, *et al*: Lactylation: novel epigenetic regulatory and therapeutic opportunities. Am J Physiol Endocrinol Metab 324: E330-E338, 2023.

13. Rho H, Terry AR, Chronis C and Hay N: Hexokinase 2-mediated gene expression via histone lactylation is required for hepatic stellate cell activation and liver fibrosis. Cell Metab 35: 1406-1423 e1408, 2023.

14. Xiong J, He J, Zhu J, *et al*: Lactylation-driven METTL3-mediated RNA m(6)A modification promotes immunosuppression of tumor-infiltrating myeloid cells. Mol Cell 82: 1660-1677 e1610, 2022.

15. Chen Y, Li P, Lin M, *et al*: Silencing of METTL3 prevents the proliferation, migration, epithelial-mesenchymal transition, and renal fibrosis of high glucose-induced HK2 cells by mediating WISP1 in m6A-dependent manner. Aging (Albany NY) 16: 1237-1248, 2024.

16. Jin J, Shang Y, Zheng S, *et al*: Exosomes as nanostructures deliver miR-204 in alleviation of mitochondrial dysfunction in diabetic nephropathy through suppressing methyltransferase-like 7A-mediated CIDEC N6-methyladenosine methylation. Aging

(Albany NY) 16: 3302-3331, 2024.

17. Liu X, Jiang L, Zeng H*, et al*: Circ-0000953 deficiency exacerbates podocyte injury and autophagy disorder by targeting Mir665-3p-Atg4b in diabetic nephropathy. Autophagy 20: 1072-1097, 2024.

18. Tang W, Zhao Y, Zhang H, Peng Y and Rui Z: METTL3 enhances NSD2 mRNA stability to reduce renal impairment and interstitial fibrosis in mice with diabetic nephropathy. BMC Nephrol 23: 124, 2022.

19. Yuan X, Wang Q, Zhao J, Xie H and Pu Z: The m6A methyltransferase METTL3 modifies Kcnk6 promoting on inflammation associated carcinogenesis is essential for colon homeostasis and defense system through histone lactylation dependent YTHDF2 binding. Int Rev Immunol: 1-16, 2024.

20. Jiang L, Liu X, Hu X*, et al*: METTL3-mediated m(6)A modification of TIMP2 mRNA promotes podocyte injury in diabetic nephropathy. Mol Ther 30: 1721-1740, 2022.

21. Cheng S, Chen L, Ying J*, et al*: 20(S)-ginsenoside Rh2 ameliorates ATRA resistance in APL by modulating lactylation-driven METTL3. J Ginseng Res 48: 298-309, 2024.

22. Kim S, Kang SW, Joo J*, et al*: Characterization of ferroptosis in kidney tubular cell death under diabetic conditions. Cell Death Dis 12: 160, 2021.

23. Li J, Li L, Zhang Z*, et al*: Ferroptosis: an important player in the inflammatory response in diabetic nephropathy. Front Immunol 14: 1294317, 2023.

24. Chen J, Ou Z, Gao T*, et al*: Ginkgolide B alleviates oxidative stress and ferroptosis by inhibiting GPX4 ubiquitination to improve diabetic nephropathy. Biomed Pharmacother 156: 113953, 2022.

25. Pu Z, Wang W, Xie H and Wang W: Apolipoprotein C3 (ApoC3) facilitates NLRP3 mediated pyroptosis of macrophages through mitochondrial damage by accelerating of the interaction between SCIMP and SYK pathway in acute lung injury. Int Immunopharmacol 128: 111537, 2024.

26. Li L, Dai Y, Ke D*, et al*: Ferroptosis: new insight into the mechanisms of diabetic nephropathy and retinopathy. Front Endocrinol (Lausanne) 14: 1215292, 2023.

27. Liu Z, Nan P, Gong Y, Tian L, Zheng Y and Wu Z: Endoplasmic reticulum stress-triggered ferroptosis via the XBP1-Hrd1-Nrf2 pathway induces EMT progression in diabetic nephropathy. Biomed Pharmacother 164: 114897, 2023.

28. Feng AF, Liu ZH, Zhou SL, Zhao SY, Zhu YX and Wang HX: Effects of AMPD1 gene C34T polymorphism on cardiac index, blood pressure and prognosis in patients with cardiovascular diseases: a meta-analysis. BMC Cardiovasc Disord 17: 174, 2017.

29. Saab R, Zouk AN, Mastouri R, Skaar TC, Philips S and Kreutz RP: AMPD1 polymorphism and response to regadenoson. Pharmacogenomics 16: 1807-1815, 2015.

30. Wang L, Zhang X, Wang M*, et al*: AMPD1 Is Associated With the Immune Response and Serves as a Prognostic Marker in HER2-Positive Breast Cancer. Front Oncol 11: 749135, 2021.

31. Hsu CM, Chang SF, Tsai YT*, et al*: Down-regulation of AMPD3 Is Associated With Poor Survival in Head and Neck Squamous Cell Carcinoma. In Vivo 36: 704-712, 2022.

32. Cheng L, Zhu M, Xu X*, et al*: AMPD3 promotes doxorubicin-induced cardiomyopathy through HSP90α-mediated ferroptosis. iScience 27: 111005, 2024.

33. Cheng J, Morisaki H, Toyama K, Ikawa M, Okabe M and Morisaki T: AMPD3-deficient mice exhibit increased erythrocyte ATP levels but anemia not improved due to PK deficiency. Genes Cells 17: 913-922, 2012.

34. Kang S, Zhang J and Yuan Y: Abietic acid attenuates IL-1β-induced inflammation in human osteoarthritis chondrocytes. Int Immunopharmacol 64: 110-115, 2018.

35. Chen H and Lu M: Abietic Acid Alleviates the Hypoxic Injury of Cardiomyocytes by Adjusting Autophagy and Apoptosis Mediated by miR-30a-5p/GRP78 Axis. Ann Clin Lab Sci 54: 748-755, 2024.

36. de Lima Silva MG, Santos da Silva LY, Torres Pessoa R*, et al*: Antiedematogenic and Analgesic Activities of Abietic Acid in Mice. Chem Biodivers 20: e202300906, 2023.

37. Dzięgielewska M, Bartoszewicz M, Książczyk M*, et al*: Abietic Acid as a Novel Agent against Ocular Biofilms: An In Vitro and Preliminary In Vivo Investigation. Int

J Mol Sci 252024.

38. An Y, Luo Q, Han D and Guan L: Abietic acid inhibits acetaminophen-induced liver injury by alleviating inflammation and ferroptosis through regulating Nrf2/HO-1 axis. Int Immunopharmacol 118: 110029, 2023.

39. Zhang W, Yang H, Sui B*, et al*: Ophiopogonin C protects against acute lung injury by fatal sepsis through pyroptosis macrophage. Phytomedicine 142: 156698, 2025.

40. Nisa M, Naseralallah L, Altarawneh L, Ally R and Danjuma M: The Prevalence of Potentially Inappropriate Medications Among Patients With Diabetic Nephropathy: A Cross-Sectional Study Conducted at a Tertiary Care Hospital. Cureus 16: e74159, 2024.

41. Shi J, Liu X, Jiao Y*, et al*: mTOR pathway: A key player in diabetic nephropathy progression and therapeutic targets. Genes Dis 12: 101260, 2025.

42. Zhang F, Han Y, Mao Y and Li W: Associations between non-insulin-based insulin resistance indices and diabetic nephropathy in patients with diabetes mellitus in US adults: a cross-sectional study of NHANES 1999-2018. Front Endocrinol (Lausanne) 15: 1458521, 2024.

43. Varatharajan S, Jain V, Pyati AK*, et al*: Neutrophil gelatinase-associated lipocalin, kidney injury molecule-1, and periostin: Novel urinary biomarkers in diabetic nephropathy. World J Nephrol 13: 98880, 2024.

44. Song C, Wang S, Fu Z*, et al*: IGFBP5 promotes diabetic kidney disease progression by enhancing PFKFB3-mediated endothelial glycolysis. Cell Death Dis 13: 340, 2022.

45. Laustsen C, Nielsen PM, Nørlinger TS*, et al*: Antioxidant treatment attenuates lactate production in diabetic nephropathy. Am J Physiol Renal Physiol 312: F192-F199, 2017.

46. Azushima K, Kovalik JP, Yamaji T*, et al*: Abnormal lactate metabolism is linked to albuminuria and kidney injury in diabetic nephropathy. Kidney Int 104: 1135-1149, 2023.

47. Darshi M, Kugathasan L, Maity S*, et al*: Glycolytic lactate in diabetic kidney

disease. JCI Insight 92024.

48. Zheng T, Gu YP, Wang JM, Huang TT, Gou LS and Liu YW: Lactate-triggered histone lactylation contributes to podocyte epithelial-mesenchymal transition in diabetic nephropathy in mice. Chem Biol Interact 408: 111418, 2025.

49. Wang J, Yang P, Yu T*, et al*: Lactylation of PKM2 Suppresses Inflammatory Metabolic Adaptation in Pro-inflammatory Macrophages. Int J Biol Sci 18: 6210-6225, 2022.

50. Wang N, Wang W, Wang X*, et al*: Histone Lactylation Boosts Reparative Gene Activation Post-Myocardial Infarction. Circ Res 131: 893-908, 2022.

51. Wang X, Fan W, Li N*, et al*: YY1 lactylation in microglia promotes angiogenesis through transcription activation-mediated upregulation of FGF2. Genome Biol 24: 87, 2023.

52. Hu K, Yu Z, Yuan Y*, et al*: Lactate/AARS1/H3K18la/LDHA positive feedback loop triggers ferroptosis, which participates in diabetic nephropathy via the modulation of ACSL4 transcription. Acta Biochim Biophys Sin (Shanghai)2025.

53. Wu D, Spencer CB, Ortoga L, Zhang H and Miao C: Histone lactylation-regulated METTL3 promotes ferroptosis via m6A-modification on ACSL4 in sepsis-associated lung injury. Redox Biol 74: 103194, 2024.

54. Fu C, Jiang W, Wang C*, et al*: AP001885.4 promotes the proliferation of esophageal squamous cell carcinoma cells by histone lactylation- and NF-κB (p65)-dependent transcription activation and METTL3-mediated mRNA stability of c-myc. Anim Cells Syst (Seoul) 28: 536-550, 2024.

55. Ogawa T, Kouzu H, Osanami A*, et al*: Downregulation of extramitochondrial BCKDH and its uncoupling from AMP deaminase in type 2 diabetic OLETF rat hearts. Physiol Rep 11: e15608, 2023.

56. Mengstie MA, Seid MA, Gebeyehu NA*, et al*: Ferroptosis in diabetic nephropathy: Mechanisms and therapeutic implications. Metabol Open 18: 100243, 2023.

57. Tan H, Chen J, Li Y*, et al*: Glabridin, a bioactive component of licorice, ameliorates diabetic nephropathy by regulating ferroptosis and the VEGF/Akt/ERK

pathways. Mol Med 28: 58, 2022.

58. Wang H, Yu X, Liu D*, et al*: VDR Activation Attenuates Renal Tubular Epithelial Cell Ferroptosis by Regulating Nrf2/HO-1 Signaling Pathway in Diabetic Nephropathy. Adv Sci (Weinh) 11: e2305563, 2024.

59. Wei M, Liu X, Tan Z, Tian X, Li M and Wei J: Ferroptosis: a new strategy for Chinese herbal medicine treatment of diabetic nephropathy. Front Endocrinol (Lausanne) 14: 1188003, 2023.

60. Ma X, Chen A, Melo L*, et al*: Loss of hepatic DRP1 exacerbates alcoholic hepatitis by inducing megamitochondria and mitochondrial maladaptation. Hepatology 77: 159-175, 2023.

61. Feng W, Wang J, Yan X*, et al*: ERK/Drp1-dependent mitochondrial fission contributes to HMGB1-induced autophagy in pulmonary arterial hypertension. Cell Prolif 54: e13048, 2021.

62. Schmitt K, Grimm A, Dallmann R*, et al*: Circadian Control of DRP1 Activity Regulates Mitochondrial Dynamics and Bioenergetics. Cell Metab 27: 657-666 e655, 2018.

63. Osanami A, Sato T, Toda Y*, et al*: Adenosine monophosphate deaminase in the endoplasmic reticulum-mitochondria interface promotes mitochondrial Ca(2+) overload in type 2 diabetes rat hearts. J Diabetes Investig 14: 560-569, 2023.

64. Kauffman ME, Kauffman MK, Traore K*, et al*: MitoSOX-Based Flow Cytometry for Detecting Mitochondrial ROS. React Oxyg Species (Apex) 2: 361-370, 2016.

65. Shadel GS and Horvath TL: Mitochondrial ROS signaling in organismal homeostasis. Cell 163: 560-569, 2015.

66. Cadenas S: Mitochondrial uncoupling, ROS generation and cardioprotection. Biochim Biophys Acta Bioenerg 1859: 940-950, 2018.

67. Zhao M, Wang Y, Li L*, et al*: Mitochondrial ROS promote mitochondrial dysfunction and inflammation in ischemic acute kidney injury by disrupting TFAM-mediated mtDNA maintenance. Theranostics 11: 1845-1863, 2021.

68. Shen S, Zhong H, Zhou X*, et al*: Advances in Traditional Chinese Medicine research in diabetic kidney disease treatment. Pharm Biol 62: 222-232, 2024.

69. Gao Y, Li Z, Wang Y*, et al*: Analysis of clinical evidence on traditional Chinese medicine for the treatment of diabetic nephropathy: a comprehensive review with evidence mapping. Front Endocrinol (Lausanne) 15: 1324782, 2024.
70. Sun J, Shen J, Liu L and Du J: The Traditional Chinese Medicine in Treating Diabetic Nephropathy: A Bibliometric Analysis. J Multidiscip Healthc 17: 4627-4636, 2024.
71. Wahab NAA, Giribabu N, Kilari EK and Salleh N: Abietic acid ameliorates nephropathy progression via mitigating renal oxidative stress, inflammation, fibrosis and apoptosis in high fat diet and low dose streptozotocin-induced diabetic rats. Phytomedicine 107: 154464, 2022.

Figure and Figure Legends

Fig. 1. Inhibition of lactate alleviates Diabetic nephropathy

Serum lactate (A), serum lactate is positively correlated with BUN, CRE, mAlb, GSH in patients with DN (B, C, D, E);

Serum lactate (F), Schematic diagram of 2-DG or oxamate (G), the experimental design of drug treatment (H), BUN (I), CRE (J), and mAlb (K), HE staining/Masson staining (L), SOD (M), MDA (N), GSH-PX (O) and GSH (P) levels in DN mice;

**p < 0.01, ***p < 0.001, and ****p < 0.001.

Fig. 2. Lactate can induce ferroptosis in Diabetic nephropathy

Pan-Kla protein expression level (A), Pan-Kla mRNA expression level (B), A score of different site Lactylation on Histone H3 and H4 (C), site-specific histone lactylation/ Histone mRNA expression level (D), H3K14la/ Kla protein expression level (E), Representative images of H3K18la co-stained with renal tubular epithelial (F) in DN mice; Pan-Kla protein and mRNA expression level (G, H).

**p < 0.01, ***p < 0.001, and ****p < 0.001.

Fig. 3. Lactate induces H3K14la increase in Diabetic nephropathy

Serum lactate is correlated with METTL3, METTL14, YTHDF1, YTHDF2, YTHDC1, YTHDC2 in patients with DN (A, B, C, D, E, F); m6A abundance of total RNA (G, H), Relative mRNA levels of m6A writers (METTL3, METTL4 and WTAP), erasers (ALKBH5 and FTO) and readers (YTHDF1, YTHDF2, YTHDF3, YTHDC1, YTHDC2, IGF2BP1, IGF2BP2, IGF2BP3) (I), METTL3/ YTHDC1 protein expression (J, K), GPR81/ METTL3 protein expression (L), H3K18la enrichment at Mettl3 promoter by lactate or PBS for 12 h was analyzed by ChIP-qPCR in vitro

model (M), scheme depicting the lactate/H3K14la axis that upregulates METTL3 and increases m6A modification (N).

*p < 0.05, **p < 0.01, ***p < 0.001, and ****p < 0.0001.

Fig. 4. AMPD3 expression levels in DN model

Heat map (A), AMPD3 mRNA expression (B) in patients DN, AMPD3 mRNA and protein in mice model of DN (C, D), Immunohistochemistry and immunofluorescence for AMPD3 expression in mice model of DN (E, F).

***p < 0.001, and ****p < 0.0001.

Fig. 5. GPR81/METTL3/YTHDC1 axis mediates AMPD3 mRNA stability through m6A modification by METTL3

AMPD3 mRNA and protein expression (A), the predicted m6A sites of AMPD3 mRNA (B), The relative levels of m6A in AMPD3 were measured by MeRIP-qPCR (C), AMPD3 protein and mRNA level in NRK-52E cells treated by lactate for 6 h (D), AMPD3 mRNA levels were analyzed by RT-qPCR assay in si-NC, si-METTL3, or siYTHDC1 NRK-52E cells after actinomycin D treatment for 0, 2, 4, and 6 h (E), Western blotting analyses of METTL3, YTHDC1, and GPX4 in NRK-52E cells treated with lactate (F and G), Cell viability of si-METTL3 or si-YTHDC1 in NRK-52E cell treated with lactate (I and J), METTL3 and GPX4 in NRK-52E cells pretreated with CHCA after 12 h lactate treatment (K), METTL3, ACSL4, and GPX4 protein expression in 12 h-lactate stimulated NRK-52E cells pretreated with 3-OBA or transfected (L), GPR81, METTL3, ACSL4, and GPX4 protein expression in 12 h-lactate stimulated NRK-52E cells transfected with si-GPR81 (M), GPX4 expression in si-NC, si-MCT1, siGPR81, or si-MCT1 combined with si-GPR81 in NRK-52E cells with or without lactate treatment (N).

*p < 0.05, **p < 0.01, ***p < 0.001, and ****p < 0.001.

Fig. 6. Single-cell sequencing data for AMPD3 expression levels in DN model

Single-cell sequencing data for AMPD3 expression (A), AMPD3 was found to be

expressed in renal tubular epithelial (C), B cells (D), T cells (E) and macrophage (F).

Fig. 7. GPR81/METTL3/YTHDC1 axis mediates AMPD3 mRNA stability through m6A modification by METTL3

Representative images of mito-tracker staining in NRK-52E cells treated with lactate over time. (Red, mito-tracker; blue, DAPI. Bar = 200 μm) (A); ATP levels (B), mitochondrial calcium ion intensity (C), Relative mitochondria-related mRNA (Ak2, Fh1, Ndufa6, Tfam, Ppargc1a, Prc1, Atp5f1b, D, E) in lactate-treated NRK-52E cells accumulated by lactate for 0, 1, 3, 6, 12, and 24 h;

ECAR and OCR analyses of NRK-52E treated with lactate for 0, 3, 6, and 12 h by seahorse (F, G), JC-1 assay/ Mitochondria CoCl2 levels (H), Iron concentration level (I), Schematic representation of Drp1-involved intra-mitochondrial metabolism and downstream TCA cycle (J),

Western blotting analyses of AMPD3, HSP90a, p-Drp1, MCU in NRK-52E cells stimulated with lactate over time (K). Mitochondria-related mRNA of NRK-52E cells transfected with shNC or sh-METTL3 after PBS or lactate treatment for 6 h (L).

AMPD3, HSP90a, p-Drp1, GPX4 protein expression in sh-NC or sh-METTL3 in NRK-52E cells after lactate treatment (M).

JC-1 assay/ Mitochondria CoCl2 levels, Iron concentration level in sh-NC or sh-METTL3 in NRK-52E cells after lactate treatment (N, O, P).

Electron microscope (Q)

Representative immunofluorescence images of C11 BODIPY staining in sh-NC or sh-METTL3 NRK-52E cells after lactate stimulation (R).

*$p < 0.05$, **$p < 0.01$, ***$p < 0.001$, and ****$p < 0.001$.

Fig. 8. Sh-AMPD3 reduced HSP90a/Drp1 to promote ferroptosis in model of DN

Kidney-to-body weight ratio (A), water intake (B), serum creatinine levels (C), urinary nitrogen (D), urinary albumin excretion (E), E-cadherin mRNA (F), and reduced periostin mRNA levels (G), MDA level (H), SOD/ GSH-PX /GSH/ levels (I, J, K), Ferrous iron levels (L), AMPD3/HSP90a/p-Drp1/GPX4 protein expression (M),

HE staining (N) in mice model of DN;

AMPD3/HSP90a/p-Drp1/GPX4 protein expression (O), GSH/ levels (P), MDA level (Q), JC-1 assay (R), Iron concentration level (S) in vitro model of DN by AMPD3 up-regulation;

AMPD3/HSP90a/p-Drp1/GPX4 protein expression (T), GSH/ levels (U), MDA level (V), JC-1 assay (W), Iron concentration level (X) in vitro model of DN by AMPD3 down-regulation;

*$p < 0.05$, **$p < 0.01$, ***$p < 0.001$, and ****$p < 0.001$.

Fig. 9. AMPD3 interacted with HSP90a by promoting its K63-linked polyubiquitination and proteasomal degradation

Immunofluorescence for AMPD3 and HSP90a in vitro model of DN (A), Immunofluorescence and immunohistochemistry for AMPD3 and HSP90a in mice model of DN (B), IP for AMPD3 and HSP90a by Lactate (C), HSP90a protein ubiquitination (D, E), 3D/IP assay for AMPD3 protein interlinking with HSP90a protein (F, G, H).

Fig. 10. Screening of potential compounds that can target AMPD3

Experimental schematic diagram (A), the structural diagram of AA (B), 3D assay for AMPD3 protein interlinking with AA (C), AMPD3 mRNA expression (D), TSA in the presence or absence of AMPD3 and AA (E), The thermal stability of plasmids encoding WT- AMPD3 and Mut- AMPD3 after treatment with AA was assessed using CETSA (F, G, H), ubiquitination AMPD3 (I), RMSD/ Hbond number/ RMSF/ Molecular Docking (Root Mean Square Deviation, J), the binding of AA to recombinant human AMPD3 proteins (surface plasmon resonance (SPR), K).

Fig. 11. AA Targeting AMPD3 alleviates DN through ferroptosis by mitochondrial fragmentation

AMPD3/ HSP90a/p-Drp1 protein expression (A), HE/Masson staining (B), Kidney-to-body weight ratio (C), water intake (D), urinary nitrogen (E), MDA level

(F), GSH/ levels (G) in mice model of DN;

AMPD3/ HSP90a/p-Drp1 protein expression (H), MDA level (I), GSH/ levels (J), Iron concentration level (K) in vitro model of DN.

*p < 0.05, **p < 0.01, ***p < 0.001, and ****p < 0.001.

Fig. 12. AA reduced the interaction between the interconnection of AMPD3 and HIF1α

The pulling-down with streptavidin magnetic beads for AMPD3 (A, B, C); the cellular location of AMPD3 and Biotin-AA was examined by immunofluorescence staining in NRK-52E cell (D);

Bioluminescence imaging for AA in lung tissue (E); Bioluminescence imaging for AA (F). IP showed that the interaction between FASN and HIF1α protein expressions (G). IP, Immunoprecipitation.

Fig. 13. Histone lactylation-regulated m6A-methylase METTL3 accelerates AMPD3-induced ferroptosis in Diabetic nephropathy

Fig. 1

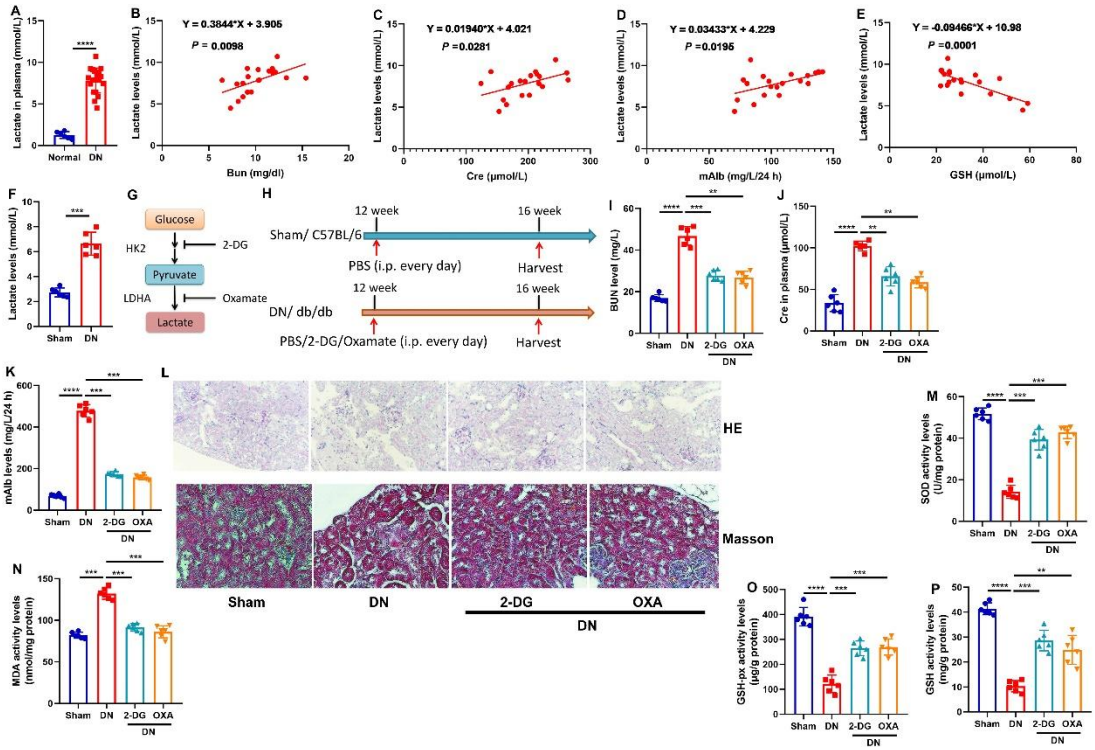
A
Lactate in plasma (mmol/L)
Normal
DN
B
Y = 0.3844*X + 3.905
P = 0.0098
Lactate levels (mmol/L)
Bun (mg/dl)
C
Y = 0.01940*X + 4.021
P =0.0281
Cre (μmol/L)
D
Y = 0.03433*X + 4.229
P =0.0195
mAlb (mg/L/24 h)
E
Y = -0.09466*X + 10.98
P =0.0001
GSH (μmol/L)
F
Sham
DN
G
Glucose
HK2
2-DG
Pyruvate
LDHA
Oxamate
Lactate
H
12 week
16 week
Sham/ C57BL/6
PBS (i.p. every day)
Harvest
DN/ db/db
PBS/2-DG/Oxamate (i.p. every day)
I
BUN level (mg/L)
J
Cre in plasma (μmol/L)
K
mAlb levels (mg/L/24 h)
L
HE
Masson
Sham
DN
2-DG
OXA
M
SOD activity levels (U/mg protein)
N
MDA activity levels (nmol/mg protein)
O
GSH-px activity levels (μg/g protein)
P
GSH activity levels (mg/g protein)

Fig. 2

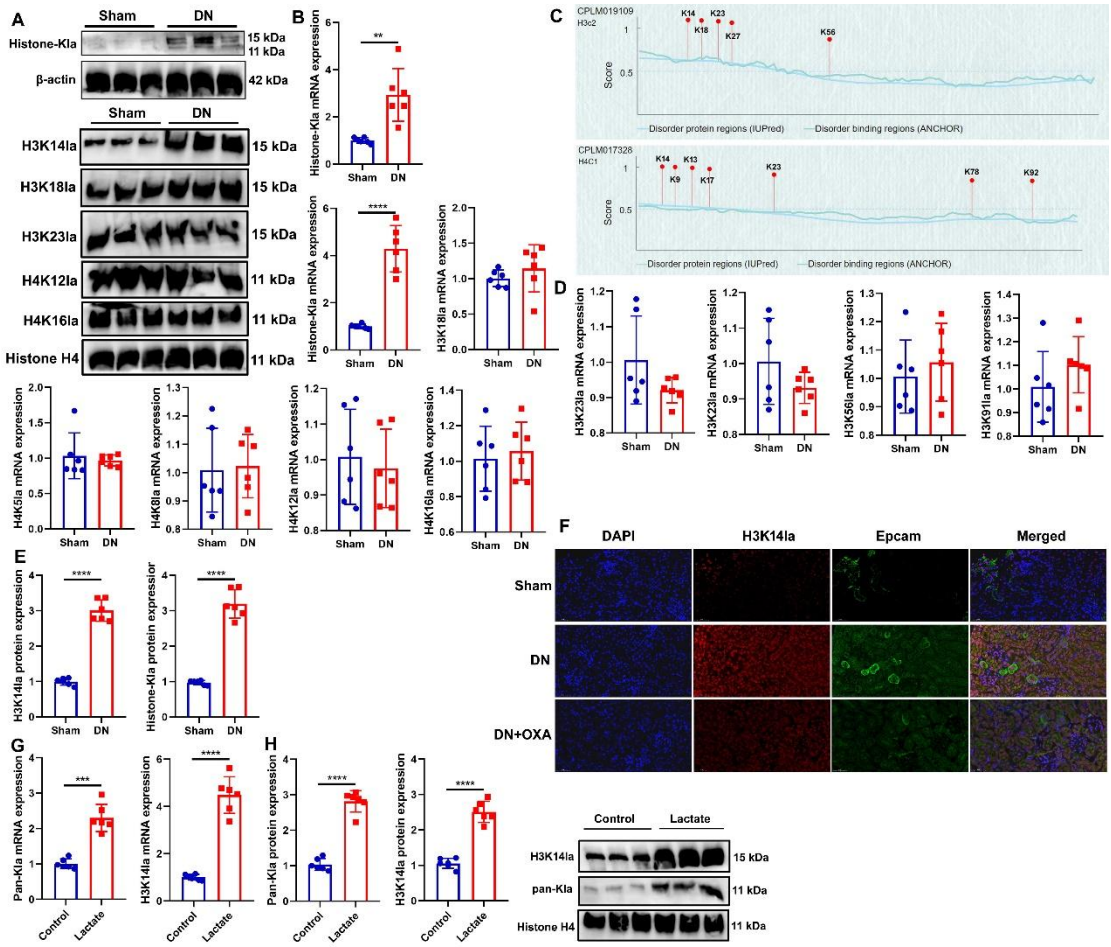
A
Sham
DN
Histone-Kla
15 kDa
11 kDa
β-actin
42 kDa
H3K14la
H3K18la
H3K23la
H4K12la
H4K16la
Histone H4
15 kDa
11 kDa
B
Histone-Kla mRNA expression
H3K18la mRNA expression
H4K5la mRNA expression
H4K8la mRNA expression
H4K12la mRNA expression
H4K16la mRNA expression
C
CPLM019109
H3c2
CPLM017326
H4C1
Score
Disorder protein regions (IUPred)
Disorder binding regions (ANCHOR)
D
H3K23la mRNA expression
H3K23la mRNA expression
H3K56la mRNA expression
H3K91la mRNA expression
E
H3K14la protein expression
Histone-Kla protein expression
F
DAPI
H3K14la
Epcam
Merged
Sham
DN
DN+OXA
G
Pan-Kla mRNA expression
H3K14la mRNA expression
H
Pan-Kla protein expression
H3K14la protein expression
Control
Lactate
H3K14la
pan-Kla
Histone H4
15 kDa
11 kDa
11 kDa

Fig. 3

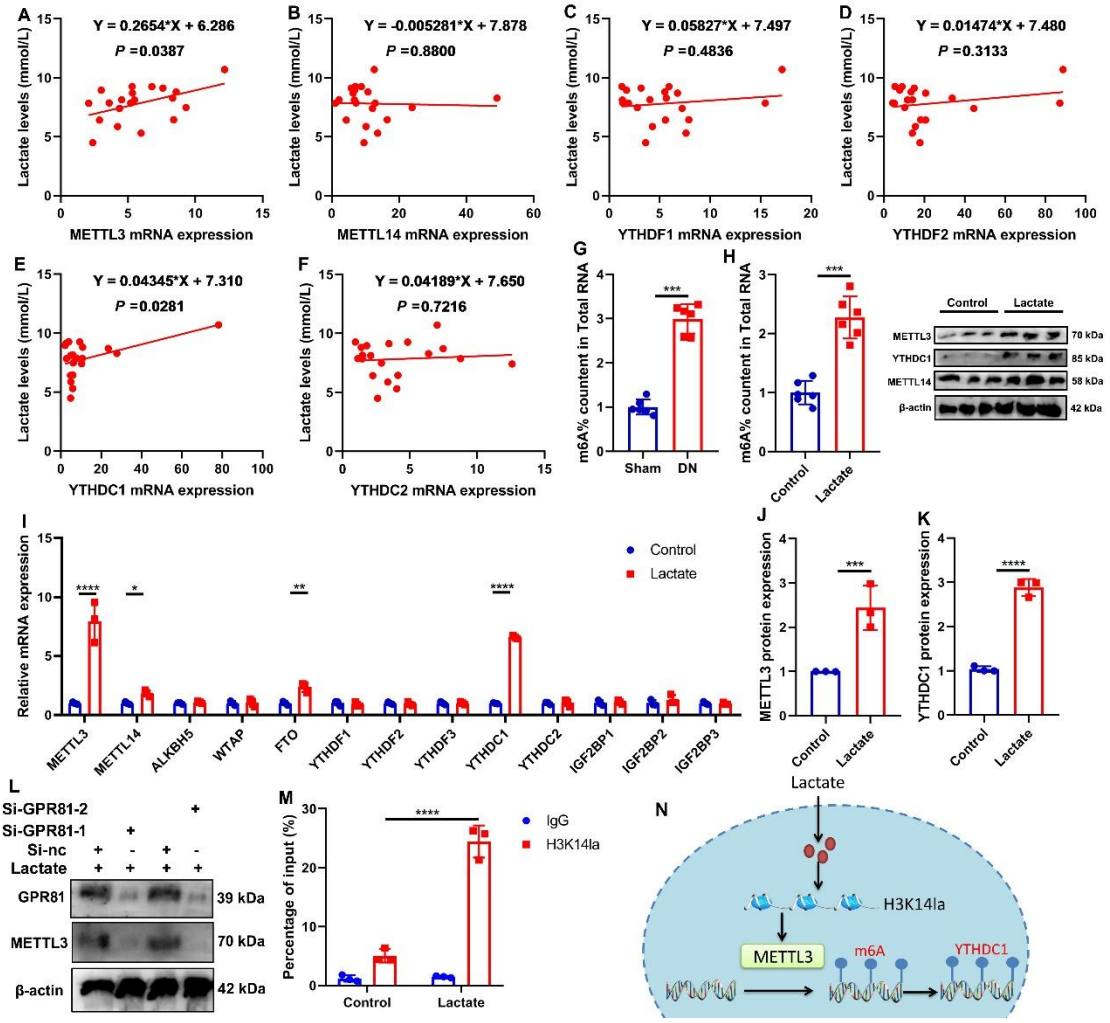
A
Y = 0.2654*X + 6.286
P =0.0387
Lactate levels (mmol/L)
METTL3 mRNA expression
B
Y = -0.005281*X + 7.878
P =0.8800
METTL14 mRNA expression
C
Y = 0.05827*X + 7.497
P =0.4836
YTHDF1 mRNA expression
D
Y = 0.01474*X + 7.480
P =0.3133
YTHDF2 mRNA expression
E
Y = 0.04345*X + 7.310
P =0.0281
YTHDC1 mRNA expression
F
Y = 0.04189*X + 7.650
P =0.7216
YTHDC2 mRNA expression
G
m6A% countent in Total RNA
Sham
DN
H
m6A% countent in Total RNA
Control
Lactate
Control
Lactate
METTL3
YTHDC1
METTL14
β-actin
70 kDa
85 kDa
58 kDa
42 kDa
I
Relative mRNA expression
Control
Lactate
METTL3
METTL14
ALKBH5
WTAP
FTO
YTHDF1
YTHDF2
YTHDF3
YTHDC1
YTHDC2
IGF2BP1
IGF2BP2
IGF2BP3
J
METTL3 protein expression
Control
Lactate
K
YTHDC1 protein expression
Control
Lactate
L
Si-GPR81-2
Si-GPR81-1
Si-nc
Lactate
GPR81
METTL3
β-actin
39 kDa
70 kDa
42 kDa
M
Percentage of input (%)
IgG
H3K14la
Control
Lactate
N
Lactate
H3K14la
METTL3
m6A
YTHDC1

Fig. 4

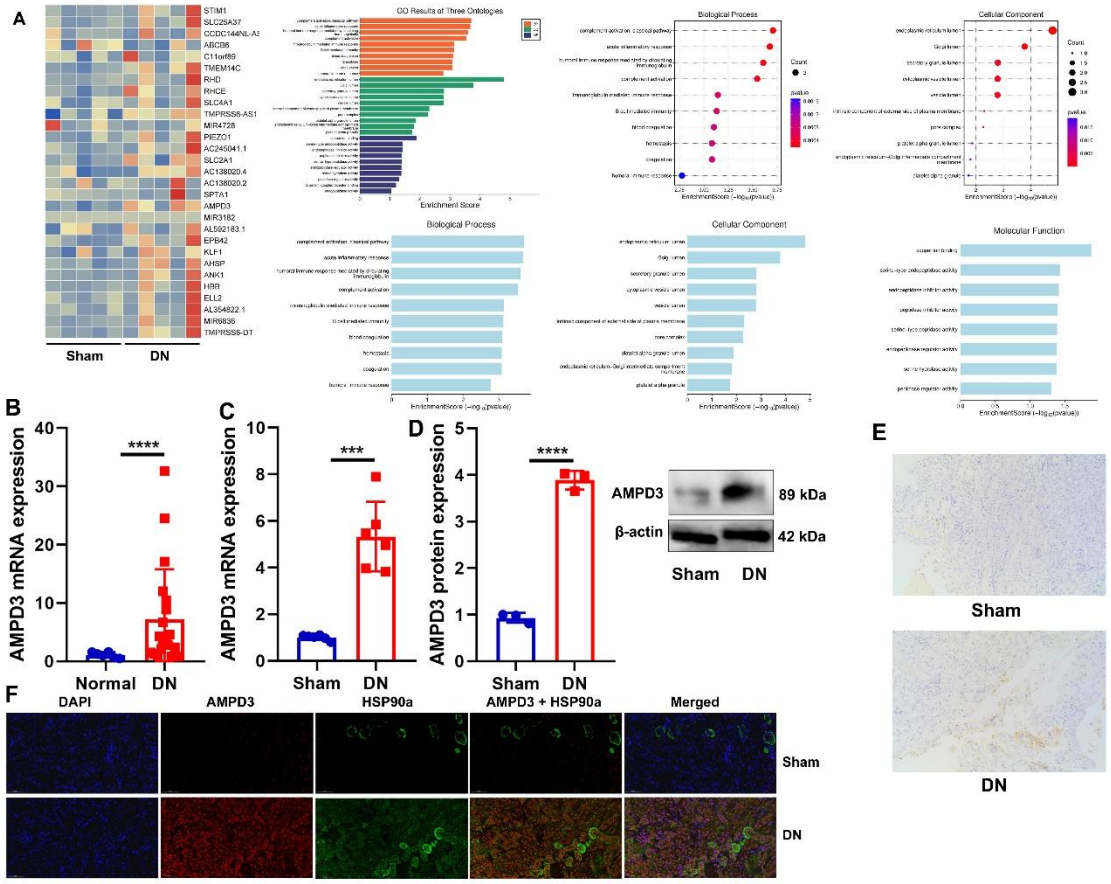
A
STIM1
SLC25A37
CCDC144NL-AS1
ABCB6
C11orf68
TMEM14C
RHD
RHCE
SLC4A1
TMPRSS6-AS1
MIR4728
PIEZO1
AC245041.1
SLC2A1
AC138020.4
AC138020.2
SPTA1
AMPD3
MIR3162
AL592183.1
EPB42
KLF1
AHSP
ANK1
HBB
ELL2
AL354822.1
MIR6836
TMPRSS6-DT
Sham
DN
GO Results of Three Ontologies
Enrichment Score
Biological Process
Cellular Component
Molecular Function
B
AMPD3 mRNA expression
****
Normal
DN
C
AMPD3 mRNA expression
***
Sham
DN
D
AMPD3 protein expression
****
Sham
DN
AMPD3
89 kDa
β-actin
42 kDa
Sham
DN
E
Sham
DN
F
DAPI
AMPD3
HSP90a
AMPD3 + HSP90a
Merged
Sham
DN

Fig. 5

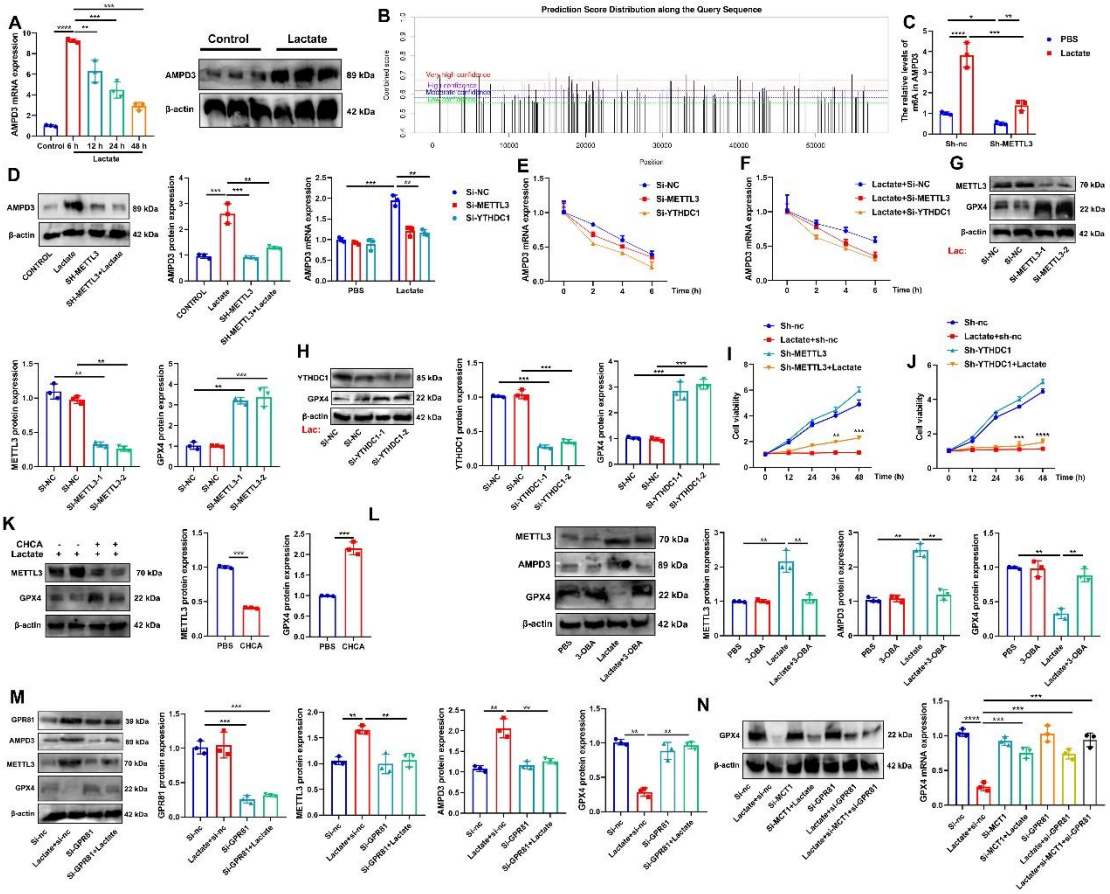
A
AMPD3 mRNA expression
Control 6 h
12 h
24 h
48 h
Lactate
Control
Lactate
AMPD3
β-actin
89 kDa
42 kDa
B
Prediction Score Distribution along the Query Sequence
Combined score
Very high confidence
High confidence
Moderate confidence
Low confidence
Position
C
PBS
Lactate
The relative levels of m6A in AMPD3
Sh-nc
Sh-METTL3
D
AMPD3
β-actin
89 kDa
42 kDa
CONTROL
Lactate
SH-METTL3
SH-METTL3+Lactate
AMPD3 protein expression
Si-NC
Si-METTL3
Si-YTHDC1
PBS
Lactate
AMPD3 mRNA expression
E
Si-NC
Si-METTL3
Si-YTHDC1
Time (h)
F
Lactate+Si-NC
Lactate+Si-METTL3
Lactate+Si-YTHDC1
Time (h)
G
METTL3
GPX4
β-actin
70 kDa
22 kDa
42 kDa
Lac:
Si-NC
Si-METTL3-1
Si-METTL3-2
METTL3 protein expression
GPX4 protein expression
H
YTHDC1
GPX4
β-actin
85 kDa
22 kDa
42 kDa
Lac:
Si-NC
Si-YTHDC1-1
Si-YTHDC1-2
YTHDC1 protein expression
I
Sh-nc
Lactate+sh-nc
Sh-METTL3
Sh-METTL3+Lactate
Cell viability
Time (h)
J
Sh-nc
Lactate+sh-nc
Sh-YTHDC1
Sh-YTHDC1+Lactate
Cell viability
Time (h)
K
CHCA
Lactate
METTL3
GPX4
β-actin
70 kDa
22 kDa
42 kDa
PBS
CHCA
L
METTL3
AMPD3
GPX4
β-actin
70 kDa
89 kDa
22 kDa
42 kDa
PBS
3-OBA
Lactate
Lactate+3-OBA
M
GPR81
AMPD3
METTL3
GPX4
β-actin
39 kDa
89 kDa
70 kDa
22 kDa
42 kDa
Si-nc
Lactate+si-nc
Si-GPR81
Si-GPR81+Lactate
GPR81 protein expression
N
GPX4
β-actin
22 kDa
42 kDa
Si-nc
Lactate+si-nc
Si-MCT1
Si-MCT1+Lactate
Si-GPR81
Lactate+si-GPR81
Lactate+si-MCT1+si-GPR81
GPX4 mRNA expression

Fig. 6

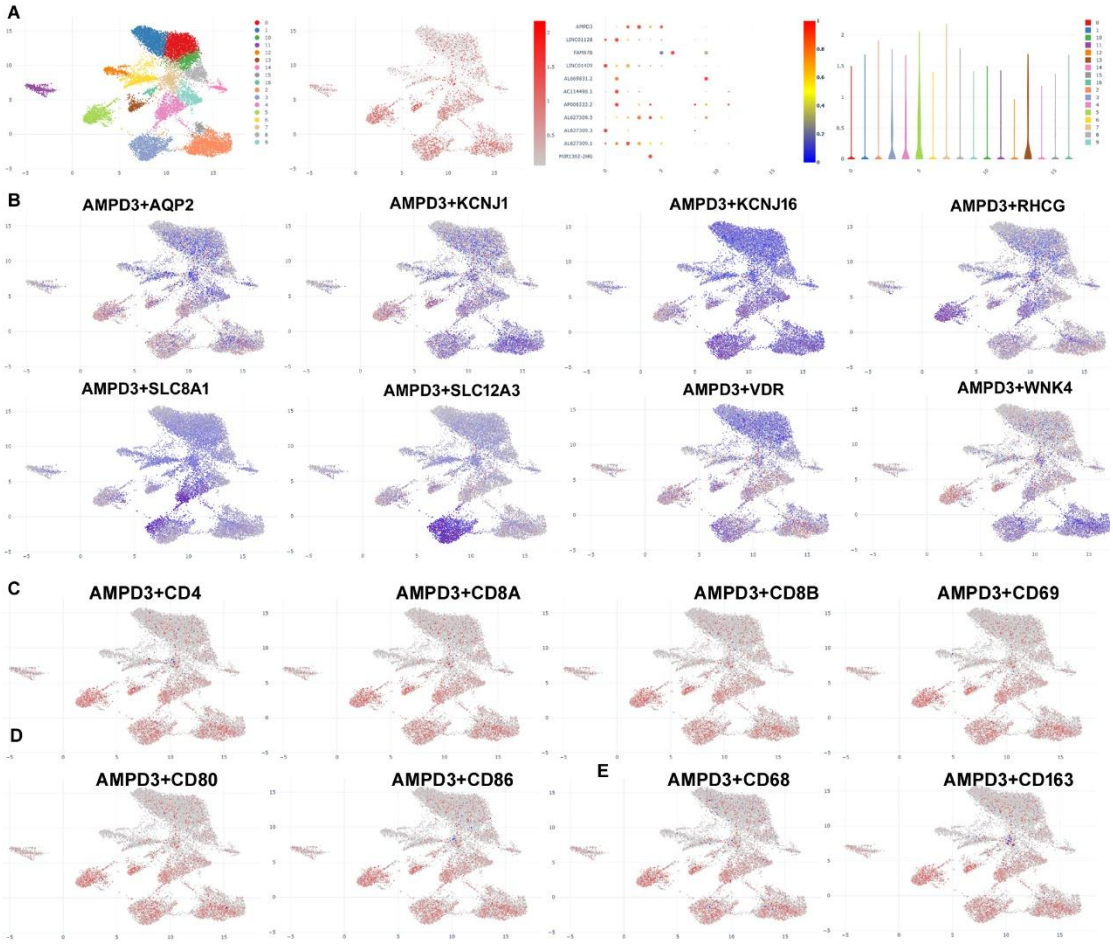
A
B
AMPD3+AQP2
AMPD3+KCNJ1
AMPD3+KCNJ16
AMPD3+RHCG
AMPD3+SLC8A1
AMPD3+SLC12A3
AMPD3+VDR
AMPD3+WNK4
C
AMPD3+CD4
AMPD3+CD8A
AMPD3+CD8B
AMPD3+CD69
D
AMPD3+CD80
AMPD3+CD86
E
AMPD3+CD68
AMPD3+CD163

Fig. 7

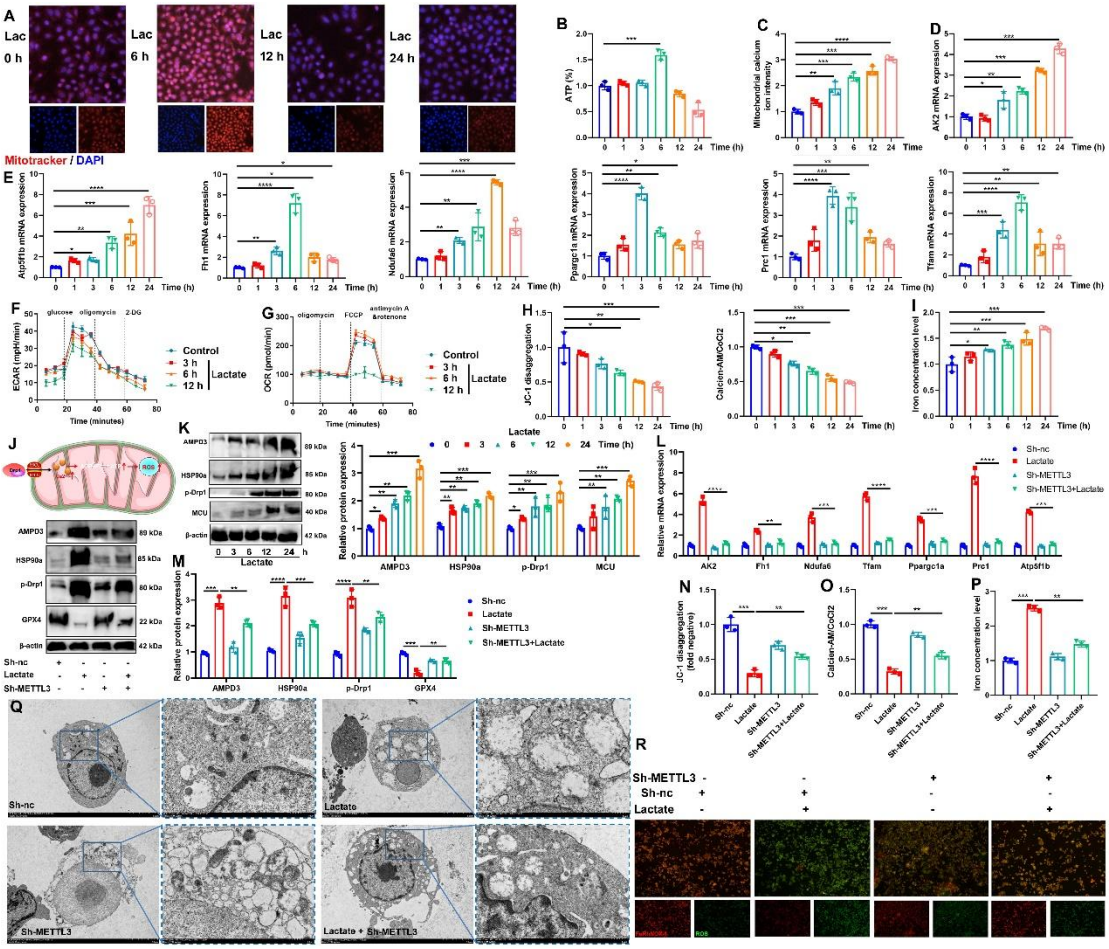
A
Lac 0 h
Lac 6 h
Lac 12 h
Lac 24 h
Mitotracker / DAPI
B
ATP (%)
C
Mitochondrial calcium ion influxion
D
AK2 mRNA expression
E
Atp5f1b mRNA expression
Fh1 mRNA expression
Ndufa6 mRNA expression
Ppargc1a mRNA expression
Prc1 mRNA expression
Tfam mRNA expression
Time (h)
F
glucose
oligomycin
2-DG
ECAR (mpH/min)
Time (minutes)
Control
3 h
6 h
12 h
Lactate
G
oligomycin
FCCP
antimycin A &rotenone
OCR (pmol/min)
H
JC-1 disaggregation
Calcein-AM/CoCl2
I
Iron concentration level
J
ROS
AMPD3
HSP90a
p-Drp1
GPX4
β-actin
Sh-nc
Lactate
Sh-METTL3
K
MCU
Relative protein expression
L
Relative mRNA expression
Sh-METTL3+Lactate
M
N
O
P
Q
Sh-METTL3+Lactate
R

Fig. 8

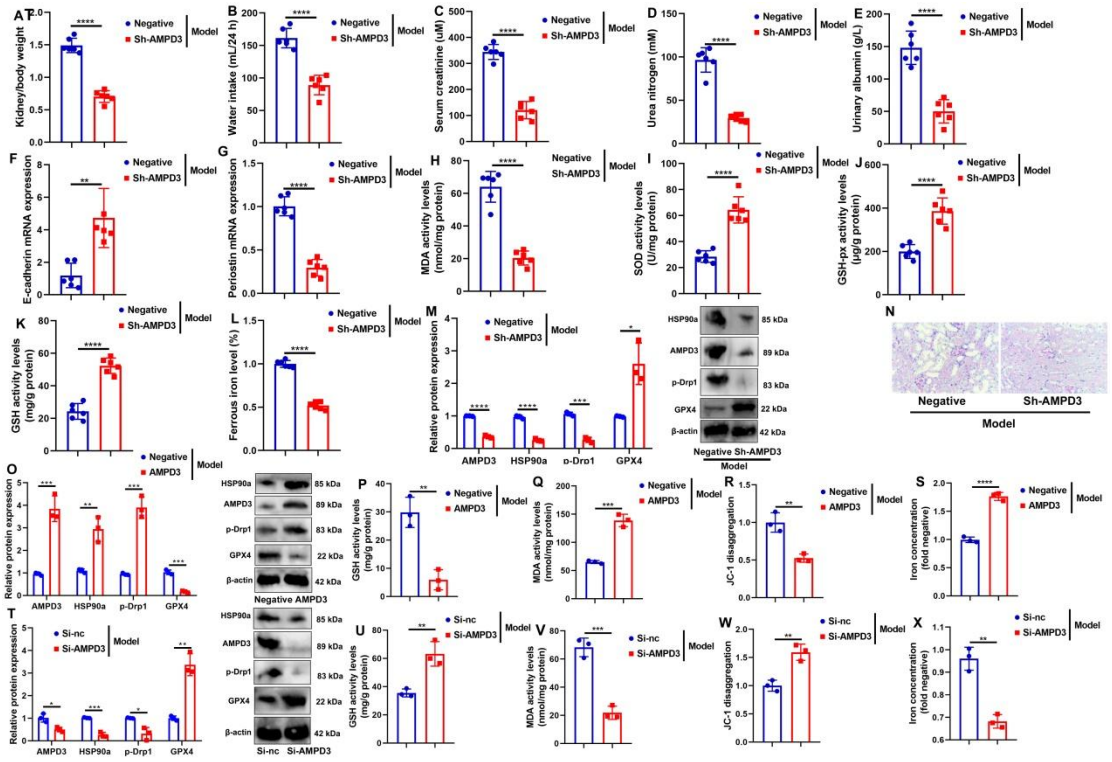
A
Kidney/body weight
B
Water intake (mL/24 h)
C
Serum creatinine (uM)
D
Urea nitrogen (mM)
E
Urinary albumin (g/L)
F
E-cadherin mRNA expression
G
Periostin mRNA expression
H
MDA activity levels (nmol/mg protein)
I
SOD activity levels (U/mg protein)
J
GSH-px activity levels (μg/g protein)
K
GSH activity levels (mg/g protein)
L
Ferrous iron level (%)
M
Relative protein expression
N
Negative
Sh-AMPD3
Model
AMPD3
HSP90a
p-Drp1
GPX4
β-actin
85 kDa
89 kDa
83 kDa
22 kDa
42 kDa
O
P
Q
R
S
T
U
V
W
X
Si-nc
Si-AMPD3
JC-1 disaggregation
Iron concentration (fold negative)

Fig. 9

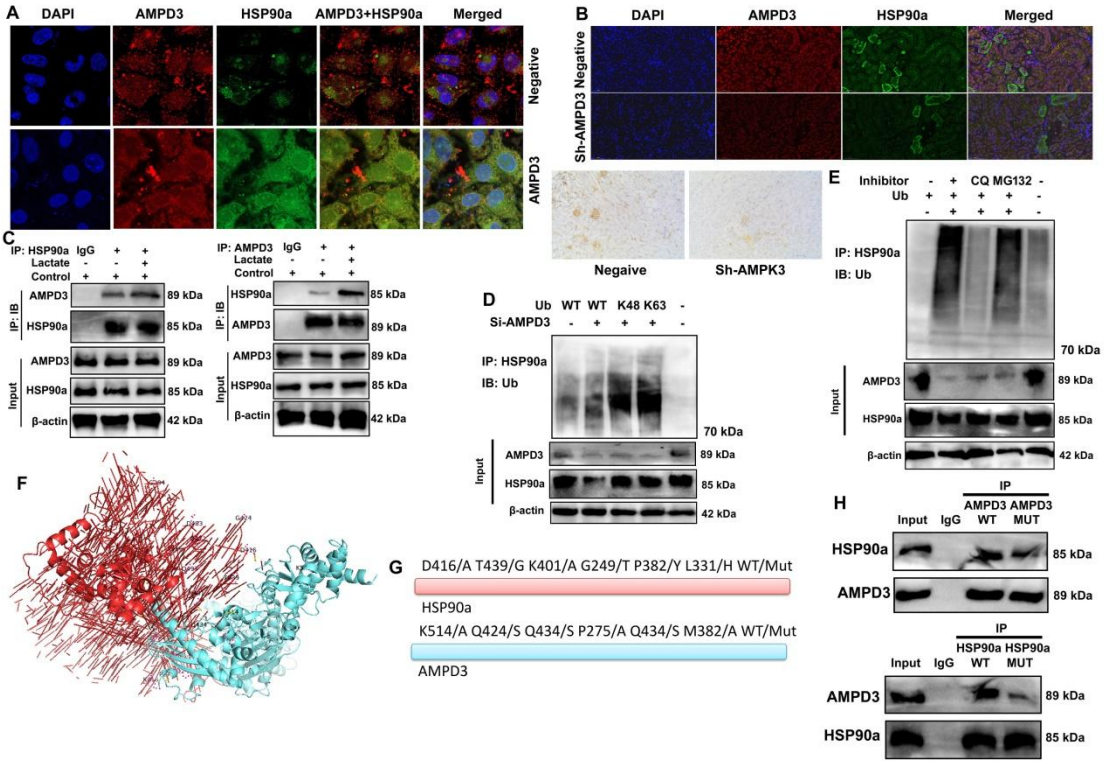
A
DAPI
AMPD3
HSP90a
AMPD3+HSP90a
Merged
Negative
AMPD3
B
DAPI
AMPD3
HSP90a
Merged
Sh-AMPD3 Negative
Negaive
Sh-AMPK3
C
IP: HSP90a IgG + +
Lactate - - +
Control + + +
IP: IB
AMPD3 89 kDa
HSP90a 85 kDa
Input
AMPD3 89 kDa
HSP90a 85 kDa
β-actin 42 kDa
IP: AMPD3 IgG + +
Lactate - - +
Control + + +
IP: IB
HSP90a 85 kDa
AMPD3 89 kDa
Input
AMPD3 89 kDa
HSP90a 85 kDa
β-actin 42 kDa
D
Ub WT WT K48 K63 -
Si-AMPD3 - + + + -
IP: HSP90a
IB: Ub
70 kDa
Input
AMPD3 89 kDa
HSP90a 85 kDa
β-actin 42 kDa
E
Inhibitor - + CQ MG132 -
Ub + + + + -
- + + + -
IP: HSP90a
IB: Ub
70 kDa
Input
AMPD3 89 kDa
HSP90a 85 kDa
β-actin 42 kDa
F
G
D416/A T439/G K401/A G249/T P382/Y L331/H WT/Mut
HSP90a
K514/A Q424/S Q434/S P275/A Q434/S M382/A WT/Mut
AMPD3
H
IP
Input IgG AMPD3 WT AMPD3 MUT
HSP90a 85 kDa
AMPD3 89 kDa
IP
Input IgG HSP90a WT HSP90a MUT
AMPD3 89 kDa
HSP90a 85 kDa

Fig. 10

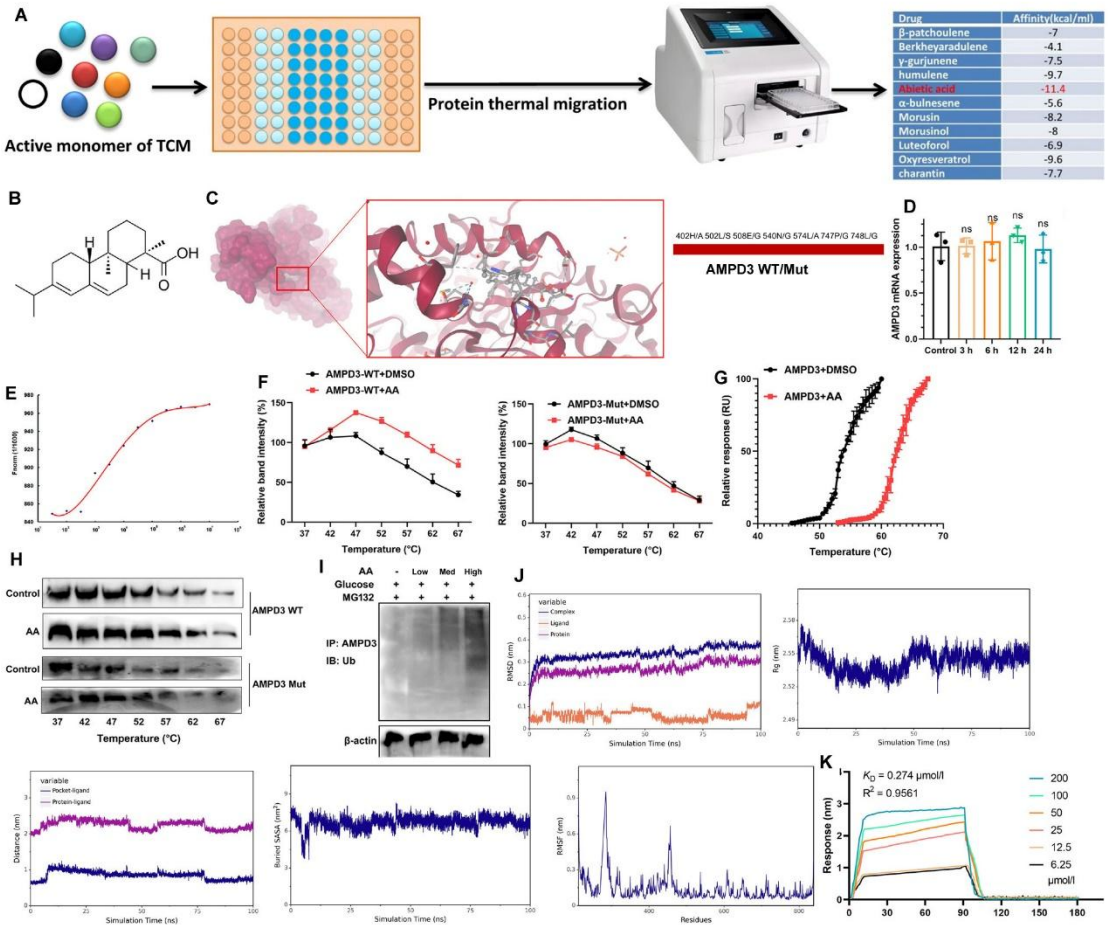
A
Active monomer of TCM
Protein thermal migration
Drug | Affinity(kcal/ml)
β-patchoulene | -7
Berkheyaradulene | -4.1
γ-gurjunene | -7.5
humulene | -9.7
Abietic acid | -11.4
α-bulnesene | -5.6
Morusin | -8.2
Morusinol | -8
Luteoforol | -6.9
Oxyresveratrol | -9.6
charantin | -7.7
B
C
402H/A 502L/S 508E/G 540N/G 574L/A 747P/G 748L/G
AMPD3 WT/Mut
D
AMPD3 mRNA expression
Control 3 h 6 h 12 h 24 h
E
F
AMPD3-WT+DMSO
AMPD3-WT+AA
AMPD3-Mut+DMSO
AMPD3-Mut+AA
Relative band intensity (%)
Temperature (°C)
G
AMPD3+DMSO
AMPD3+AA
Relative response (RU)
H
Control
AA
AMPD3 WT
AMPD3 Mut
I
AA - Low Med High
Glucose
MG132
IP: AMPD3
IB: Ub
β-actin
J
Simulation Time (ns)
K
K_D = 0.274 μmol/l
R^2 = 0.9561
Response (nm)
200
100
50
25
12.5
6.25
μmol/l

Fig. 11

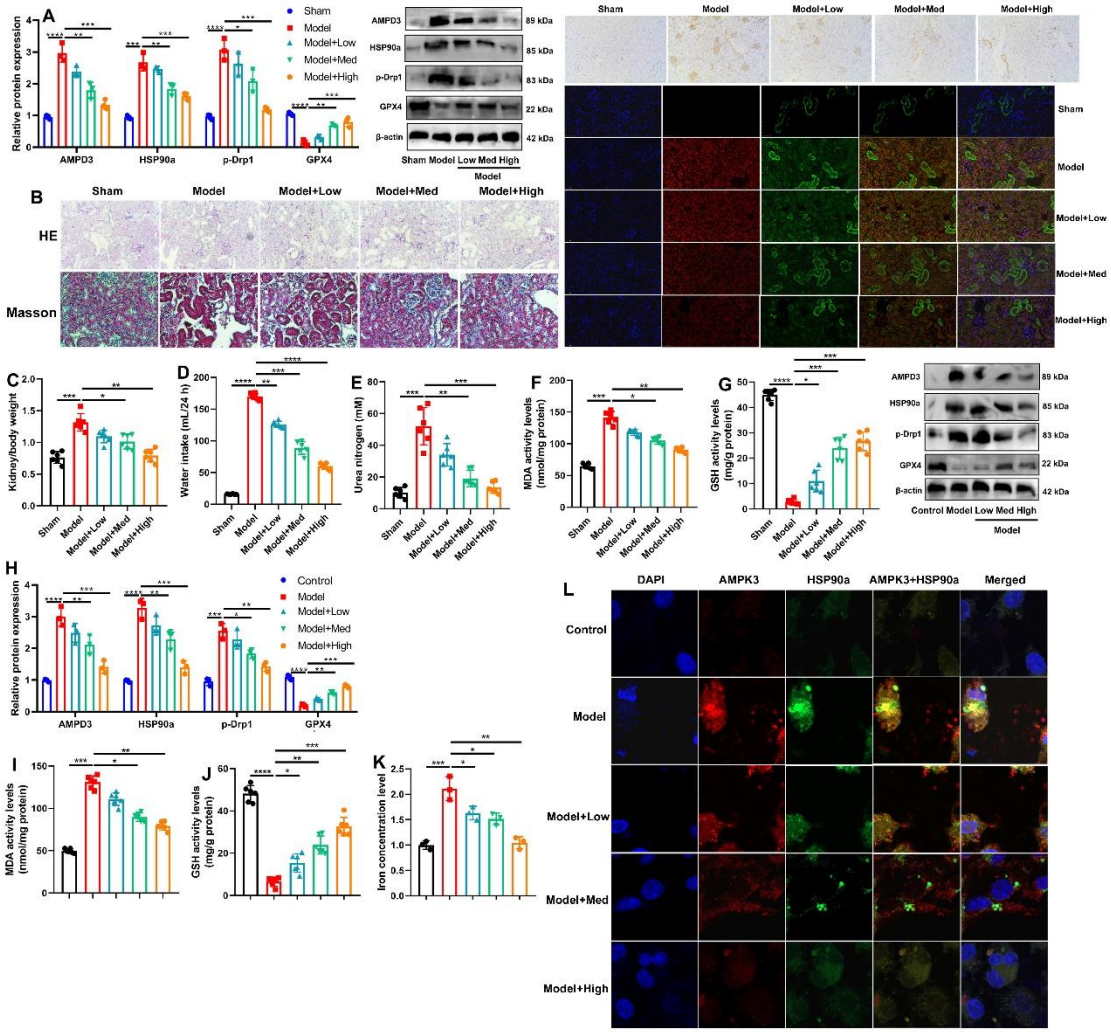
A
Relative protein expression
AMPD3
HSP90a
p-Drp1
GPX4
Sham
Model
Model+Low
Model+Med
Model+High
89 kDa
85 kDa
83 kDa
22 kDa
42 kDa
β-actin
Sham Model Low Med High
Model
B
HE
Masson
C
Kidney/body weight
D
Water intake (mL/24 h)
E
Urea nitrogen (mM)
F
MDA activity levels (nmol/mg protein)
G
GSH activity levels (mg/g protein)
H
Control
I
J
K
Iron concentration level
L
DAPI
AMPK3
HSP90a
AMPK3+HSP90a
Merged
Control
Model
Model+Low
Model+Med
Model+High

Fig. 12

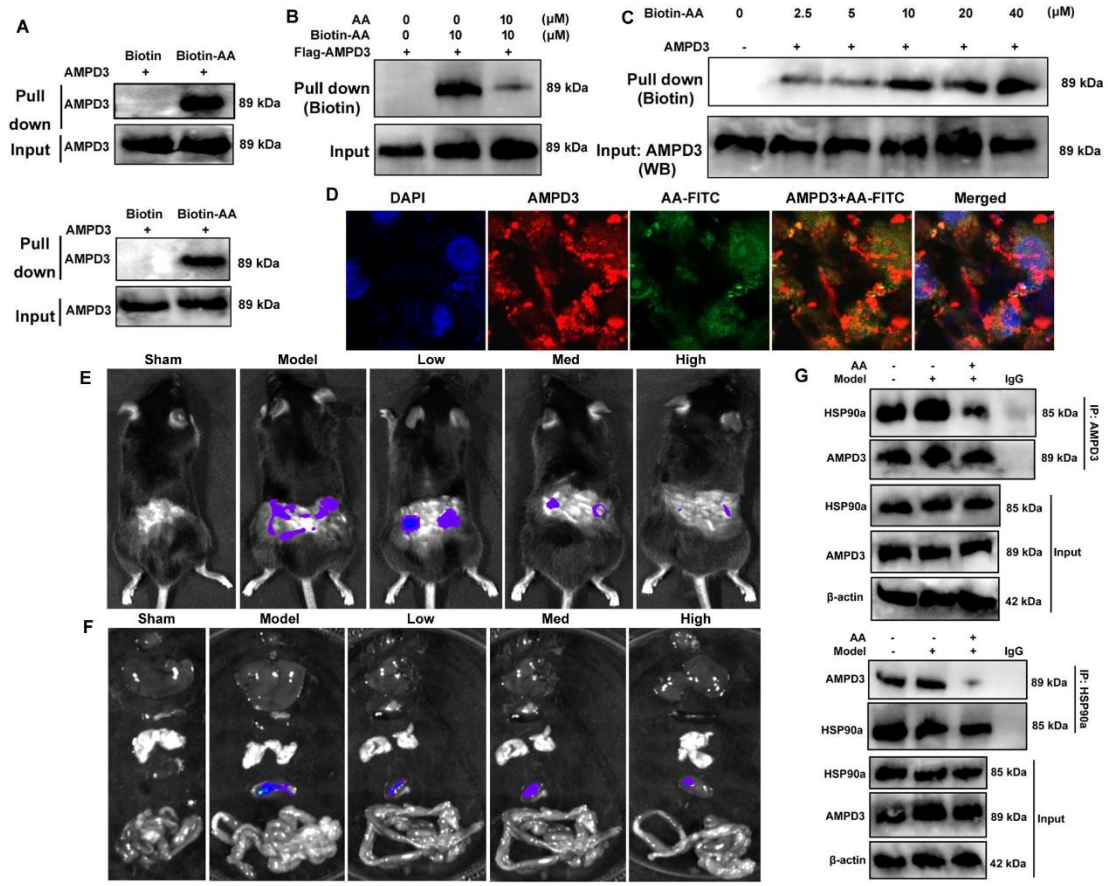
A
Biotin
Biotin-AA
AMPD3
Pull down
Input
89 kDa
B
AA
Biotin-AA
Flag-AMPD3
(μM)
Pull down (Biotin)
Input
C
Biotin-AA
AMPD3
Input: AMPD3 (WB)
D
DAPI
AMPD3
AA-FITC
AMPD3+AA-FITC
Merged
E
Sham
Model
Low
Med
High
F
G
IgG
HSP90a
β-actin
IP: AMPD3
IP: HSP90a
Input
85 kDa
42 kDa

Fig. 13

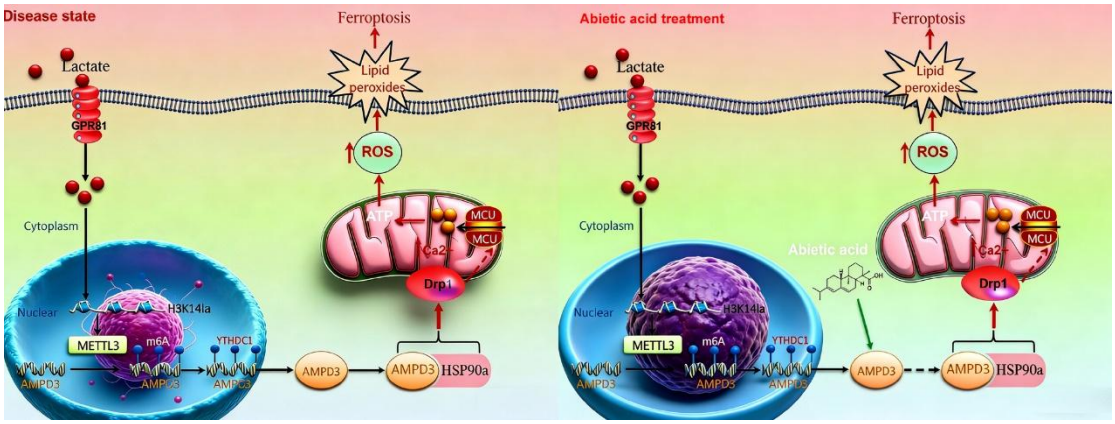
Disease state
Ferroptosis
Lactate
Lipid peroxides
GPR81
ROS
Cytoplasm
ATP
MCU
MCU
Ca2+
Drp1
Nuclear
H3K14la
METTL3
m6A
YTHDC1
AMPD3
AMPD3
AMPD3
AMPD3
AMPD3
HSP90a
Abietic acid treatment
Ferroptosis
Lactate
Lipid peroxides
GPR81
ROS
Cytoplasm
Abietic acid
ATP
MCU
MCU
Ca2+
Drp1
Nuclear
H3K14la
METTL3
m6A
YTHDC1
AMPD3
AMPD3
AMPD3
AMPD3
AMPD3
HSP90a

Supplementary Files

This is a list of supplementary files associated with this preprint. Click to download.

- WB.pdf